

NOTE TO USERS

This reproduction is the best copy available.

UMI[®]



**THERMAL ANALYSIS OF A DOUBLE GLAZED WINDOW WITH
A BETWEEN-PANES PLEATED BLIND**

by

Rasesh Dalal

B.Eng., L. E. College (India), 1998

A project

presented to Ryerson University

in partial fulfillment of the
requirement for the degree of
Master of Engineering
in the program of
Mechanical Engineering

Toronto, Ontario, Canada, 2004

© Rasesh Dalal 2004

PROPERTY OF
RYSERSON UNIVERSITY LIBRARY

UMI Number: EC52970

INFORMATION TO USERS

The quality of this reproduction is dependent upon the quality of the copy submitted. Broken or indistinct print, colored or poor quality illustrations and photographs, print bleed-through, substandard margins, and improper alignment can adversely affect reproduction.

In the unlikely event that the author did not send a complete manuscript and there are missing pages, these will be noted. Also, if unauthorized copyright material had to be removed, a note will indicate the deletion.

UMI[®]

UMI Microform EC52970

Copyright 2008 by ProQuest LLC.

All rights reserved. This microform edition is protected against unauthorized copying under Title 17, United States Code.

ProQuest LLC
789 E. Eisenhower Parkway
PO Box 1346
Ann Arbor, MI 48106-1346

BORROWER'S PAGE

Ryerson University requires the signature of all persons using or photocopying this thesis. Please sign below, and give address and date.

**THERMAL ANALYSIS OF A DOUBLE GLAZED WINDOW WITH A
BETWEEN-PANES PLEATED BLIND**

Rasesh Dalal

Master of Engineering, 2004

Department of Mechanical & Industrial Engineering

Ryerson University, Toronto, Ontario, Canada, 2004

ABSTRACT

A simplified two-dimensional numerical model of a window with a between-panes pleated blind has been developed using commercial computational fluid dynamics software. Knowledge of the effect of blinds on the free convection is important for understanding and predicting the impact of shading devices on the overall thermal performance of a window. Numerical results have been obtained for three fill gases (air, argon and krypton) and several blind geometries over the Rayleigh number range $10^3 \leq Ra \leq 10^5$. The results show that pleated blinds can have a strong effect on window thermal performance. In addition, it has been shown that the data from a convection-only model can be combined with a simplified one-dimensional model to estimate the overall U-value of the enclosure. Using this procedure, the convection data can be applied to a window/blind assembly with arbitrary radiation parameters.

ACKNOWLEDGEMENTS

The author expresses a sincere gratitude to the people who do science with pure, unselfish and honest passion, as they are the people who made him grow and appreciate the world.

The author would like to express his gratitude to all those who gave the possibility to complete this project. The author extends his sincere gratitude to many people who made this project possible.

The author is so much grateful to Prof. David Naylor for the extensive discussion on the relevant materials and for his suggestions on how each result should be presented. Since many of the observations and analyses reported in this thesis have been formed during the course of informal discussion with him. The author is deeply indebted to Dr. David Naylor. He has devoted so much time and effort to teaching the author. The author would like to express his deepest appreciation to Dr. David Naylor, without his enthusiasm and persistence, this project would have not been possible.

The author would like to gratefully thank his teachers for their contributions. Special thanks are due to Dr. Greg Kawall (the best teacher the author ever had!), Dr. Kamran Behdinan, Dr. Jacob Friedman, Dr. Liping Fang, Dr. Marc Rosen for making the learning process easy.

Finally, the author would like to thank his parents, fiancée and his family members for their support and encouragement. Special thanks are due to his mother and father for their kindness, prayer and support that proved to be a major factor in personal accomplishments.

TABLE OF CONTENTS	Page
TITLE PAGE.....	i
AUTHOR'S DECLARATION.....	ii
BORROWER'S PAGE.....	iii
ABSTRACT.....	iv
ACKNOWLEDGEMENTS.....	v
TABLE OF CONTENTS.....	vi
LIST OF TABLES.....	ix
LIST OF FIGURES.....	x
NOMENCLATURE.....	xii

CHAPTER 1: INTRODUCTION AND LITERATURE REVIEW

1.1 Introduction.....	1
1.2 Literature review.....	3
1.2.1 Natural convection in tall rectangular cavities.....	5
1.2.2 Studies of the effect of blinds on window thermal performance.....	10
1.3 Problem geometry.....	13
1.4 Objective of present study.....	15

CHAPTER 2: NUMERICAL MODEL AND SOLUTION PROCEDURES

2.1 Introduction.....	16
2.2 Governing equations.....	17
2.3 Boundary conditions.....	20
2.4 Properties of different fill gases and ASHRAE design conditions	20

2.5	Grid sensitivity for convection numerical model.....	22
2.5.1	Solution validation with the bench mark solution of De Vahl Davis and Jones (1983) for a square enclosure.....	24
2.5.2	Natural convection in 2D rectangular cavity for high aspect ratio (A = 40).....	25

CHAPTER 3 : PRESENTATION OF RESULTS

3.1	Introduction.....	28
3.2	Results from the free convection CFD model.....	28
3.2.1	Effect of properties of selected gas on the convective heat transfer.....	29
3.2.2	Effects of blind conductivity on the convective heat transfer	29
3.2.3	Effects of blind width on the convective heat transfer.....	31
3.2.4	Effects of blind angle on the convective heat transfer.....	34
3.2.5	Effects of aspect ratio on the convective heat transfer	40
3.3	Numerical radiation model of the between-panes pleated blind	41
3.3.1	Simple one dimensional model of the pleated blind	41
3.3.2	Grid independency study for convection/conduction/radiation CFD model.....	47
3.3.3	Comparison of the simplified one dimensional model with the full CFD model.....	47

CHAPTER 4: CONCLUSION

4.1	Conclusions.....	51
4.2	Recommendations.....	53

APPENDIX A: - FLUENT 6.0 sample input file.....	54
APPENDIX B:- Selected data for Nusselt number and Rayleigh number for different blind geometry.....	62
REFERENCES	64

LIST OF TABLES

Table	Title	Page
Table 2.1	ASHRAE design conditions for summer and winter.....	21
Table 2.2	Grid Independency study for Case 1, Case 2 and Case 3 at $A=20, \Phi=60^{\circ}, Ra= 10^3 \leq Ra \leq 10^5$	22
Table 3.1	Conductivity of different materials suitable for a pleated blind.....	31
Table 3.2	Total and radiation heat transfer data for three different grid densities.....	47
Table 3.3	Comparison results from the simplified model and the full CFD solution for an untreated window, High-e (Case 1).....	48
Table 3.4	Comparison results of Analytical and CFD models of Full radiation model for Low-e case (Case 2).....	49
Table B1	Nusselt number data for different blind angle.....	64
Table B2	Nusselt number data for different blind width.....	64
Table B3	Nusselt number data for different filled gas.....	65
Table B4	Nusselt Number data for different aspect ratio.....	65
Table B5	Nusselt Number data for different blind conductivity.....	65

LIST OF FIGURES

Figure	Title	Page
Figure 1.1	Pleated blind between the panes of window.....	4
Figure 1.2	Natural convection in tall cavity.....	6
Figure 1.3	Heat transfer measurement data by Elsherbiny et al. (1982) and Shewen et al. (1986) for cavities with $A \geq 40$	8
Figure 1.4	Data for Elsherbiny et al. (1983) and theory of Raithby and Hollands (1977).....	9
Figure 1.5	Geometry of pleated blind inside window glazing surfaces.....	14
Figure 2.1	Three different grid densities at $\Phi=60$ for three cases.....	23
Figure 2.2	Comparison of the crude and fine meshes used for the grid sensitivity study.....	24
Figure 2.3	Comparison of bench mark solution of De Vahl Davis and Jones (1983) with the current CFD results for $A = 1$	26
Figure 2.4	Comparison of present numerical calculation for $A=40$ with the correlation of Wright (1996)	27
Figure 3.1	Effect of Rayleigh number on average Nusselt number for different filled gas	30
Figure 3.2	Effect of Rayleigh numbers on average Nusselt number for different blind conductivity.....	32
Figure 3.3	Effect of Rayleigh number on the average Nusselt number for different blind widths.....	33
Figure 3.4	Stream function contour for the blind width $S=14\text{mm}$, $S=16\text{mm}$ and $S=18\text{mm}$	35
Figure 3.5	Isotherm contours for the blind width $S=14\text{mm}$, $S=16\text{mm}$, $S=18\text{mm}$	36
Figure 3.6	Effect of Rayleigh number on the average Nusselt Number for different blind angle	37

Figure 3.7	Stream function contour for blind angle (a) $\Phi=30^{\circ}$ (b) $\Phi=45^{\circ}$ (c) $\Phi=60^{\circ}$	38
Figure 3.8	Isotherms for blind angle (a) $\Phi=30^{\circ}$ (b) $\Phi=45^{\circ}$ (c) $\Phi=60^{\circ}$	39
Figure 3.9	Effect of Rayleigh number on the average Nusselt for different Aspect Ratio.....	42
Figure 3.10	Energy balance at a control volume around the pleated blind.....	43
Figure 3.11	Resistance network for radiation heat transfer from hot wall to the blind.....	45
Figure 3.12	(a) Isotherms for low-e case (b) Stream function for low-e case.....	50

NOMENCLATURE

A	Aspect ratio
A_B	Area of blind, (m^2)
C_p	Specific heat capacity, (J/kgK)
E	Emissive power, (W/m^2)
F	View factor
g	Acceleration due to gravity, (m/s^2)
Gr	Grashof number
h	Heat transfer coefficient, (W/m^2K)
H	Height of the cavity, (m)
k	Thermal conductivity, (W/mK)
Nu	Nusselt number
P	Pressure, (N/m^2)
p'	Pressure defect, (N/m^2)
P_b	Pitch of blind, (m)
Pr	Prandtl number
q	Heat transfer rate per unit area, (W/m^2)
Q	Heat transfer, (W)
Q_{RAD}	Radiative heat transfer, (W)
Q_{CONV}	Convective heat transfer, (W)
$Q_{RAD,HB}$	Radiative heat transfer from hot-side glazing to blind, (W)
R	Thermal resistance, (K/W)
Ra	Rayleigh number

S	Width of the blind, (m)
S1	Projection length of blind width from center, (m)
S2	Half width of the cavity, (m)
t	Glazing thickness, (m)
T	Temperature, (K)
T _b	Blind temperature, (K)
T _H	Hot side glazing temperature, (K)
T _C	Cold side glazing temperature, (K)
T _m	Mean temperature, (K)
u, v	Velocity components, (m/s)
U, V	Dimensionless velocity
U-value	Thermal conductance, (W/m ² k)
W	Window width, (m)

Greek Symbols

α	Thermal diffusivity, (m ² /s)
β	Thermal expansion coefficient, (K ⁻¹)
ε	Emissivity
σ	Stefan-Boltzmann constant, (W/m ² K ⁴)
μ	Dynamic viscosity, (Ns/m ²)
ν	Kinematic viscosity, (m ² /s)
ρ	Density, (kg/m ³)
Φ	Blind angle, (degrees)
Ψ	Stream function, (m ² /s)

Subscripts

Avg	Average
B	Blind
CB	Cold surface to blind
CFD	Computational fluid dynamic
COND	Conduction
CONV	Convection
CONV, C	Convection heat transfer from cold surface
CONV, HB	Convection from hot surface to blind
CONV, BC	Convection from blind-surface to cold surface
ER	Energy rating
F	Fluid
RAD	Radiation heat transfer
RAD, C	Radiation heat transfer from cold surface
RAD, CB	Radiation heat transfer from cold surface to blind
RAD, HB	Radiation heat transfer from hot surface to blind
TOTAL	Total heat transfer from hot surface to cold surface

CHAPTER 1: INTRODUCTION AND LITERATURE REVIEW

1.1 Introduction

Fenestration systems are primarily selected for the comfort of occupants and from an aesthetic point of view. However, windows can contribute a significant portion of the energy savings in buildings. For this reason, windows have been a source of particular concern to energy researchers. As a result, many designers have explored ways of minimizing the thermal losses through windows, while preserving their lighting and psychological benefits. Among the techniques suggested for improving window performance, the use of shading devices, both internal and external, can be mentioned. Radiant or solar heat gain through windows and glass doors can increase air conditioning costs and reduce occupant comfort. The more glass a home has, especially on east, west, and south exposures, the more important it is to have some type of window shading device. For this reason, particular interest has been directed toward improving the thermal performance of windows. Therefore, in order to effectively use shading devices to minimize window heat transfer rates, a proper understanding how these devices interact with the window's heat transfer is required.

There are several products available on the market for shading windows. The most common devices include curtains, Venetian blinds, vertical blinds and roller blinds. There is significant interest in placing a blind between the panes of a double glazed window because of several advantages. Some of these advantages are:

- (i) The blind is protected from damage (such as by children, pets, etc.).

(ii) The blind does not collect dust as quickly.

(iii) It can prevent the blind from interfering with the opening and closing of the window.

Figure 1.1(a) shows a commercial pleated blind. In terms of the history of blinds, pleated blinds are relatively newcomers. Pleated blinds were born out of the standard Venetian blind, with folded fabric in place of the horizontal slats. PellaTM (one of the world's leading manufacturers for doors and windows) has recently introduced a new product, which has a pleated blind between the panes of double glazed window. These products appear to be designed based more on aesthetic appeal and occupant comfort than on thermal performance. Figure 1.1(b) shows a close-up view of a pleated blind between the panes of double glazed window. This product is manufactured by PellaTM and it is currently available on the market. The present numerical study examines the interaction of a pleated blind with the free convection heat transfer between the panes of window.

A window system is an example of multimode heat transfer, which is the subject of this project. When a pleated blind is placed inside a window glazing, three modes of heat transfer will occur: convection, conduction and radiation. Free convection occurs in the fill gas between the glazings and is driven by the outdoor/indoor temperature difference. Conduction occurs in the solid components, which includes the glazings, end spacers, and the blind. Radiation heat transfer occurs between the hot glazing and the blind, and between the cold glazing and the blind. This heat exchange occurs across the fill gas, which is normally considered transparent to thermal radiation. In the current application, all three modes of heat transfer are coupled.

Soaring international fuel prices have caused increased interest in energy efficiency. The environmental impact of energy usage has also created interest in improved energy efficiency. As each new window design comes onto the market, performance evaluation is needed. Commercial software such as VISION (Wright, 1992) and WINDOW (Finlayson et al., 1993) are widely used by North American manufacturers to determine energy rating (ER) numbers for their products.

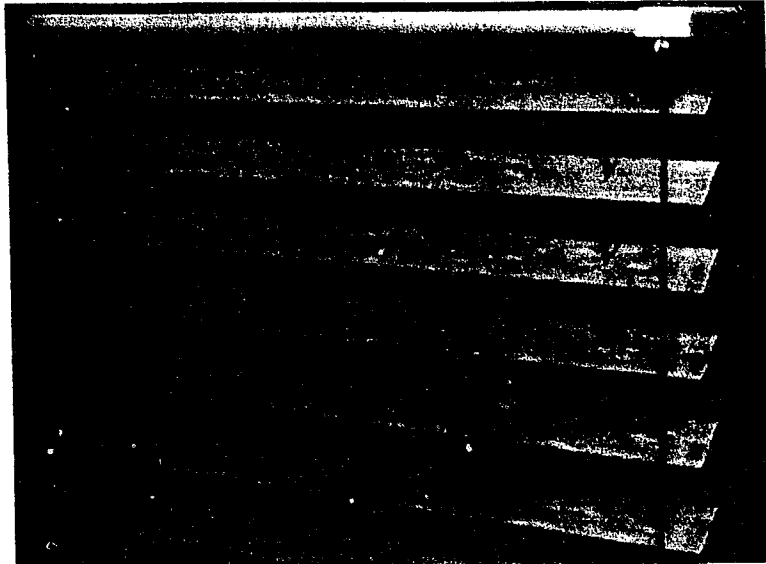
VISION and WINDOW calculate the center-glass U-Value using a simplified one-dimensional analysis. These software packages use empirical correlations for the convective heat transfer coefficients and calculate the radiation exchange using a gray-diffuse model. However, both VISION and WINDOW are restricted to the analysis of windows with no shading devices attached.

Shading devices are a vital part of a window fenestration system. In the present study, the thermal performance of a window with an inter-pane pleated blind is calculated using the CFD software FLUENT 6.0 (Fluent Inc., 1998).

1.2 Literature Review

As the name implies, inter-pane pleated blinds are located inside the window cavity. As previously mentioned, there is a free convective flow in this cavity. There has been a considerable amount of research on free convection in complex enclosures, because there are many engineering applications.

Two main areas have been reviewed that relate to this project: (i) Studies of natural convection in tall rectangular cavities, and (ii) Studies of the effects of blinds on window thermal performance.



(a)



(b)

Figure 1.1 (a) Pleated blind, (b) Pleated blind between the panes of a window.
(Images reproduced with the permission of Pella Corporation).

1.2.1 Natural Convection in Tall Rectangular Cavities

Natural convection flow and heat transfer in an air-filled vertical cavity (narrow slot) with a temperature difference maintained between the vertical walls has been under study over the past several decades (e.g., Ostrach, 1952). Such natural convection is found in many applications, such as building insulation, double-pane windows, solar collectors, and cavities surrounding the core of nuclear reactors.

Of all cavity problems, the vertical rectangular cavity is probably the most studied configuration, because of its relative simplicity and importance in many practical applications. Figure 1.2 shows a cross section of a vertical slot, which is presumed to be long in Z-direction. The temperatures of the heated wall, T_H , and cooled wall, T_C , are assumed to be uniform. Typically, the boundary conditions on the upper and lower end walls are either: (i) zero heat flux (ZHF) or (ii) linear temperature profile (LTP).

Fundamental studies and dimensional analysis have shown that the convective heat flux from the hot wall to the cold wall, q , (either local or average) can be expressed in a dimensionless form as the Nusselt number $Nu=f(Ra, Pr, A)$. For the window application, the Rayleigh number (Ra), enclosure aspect ratio (A) and Prandtl number (Pr) are given by:

$$Ra = \frac{\rho^2 W^3 g C_p \Delta T \beta}{\mu k} \quad (1.1)$$

$$A = \frac{H}{W} \quad (1.2)$$

$$Pr = \frac{\mu C_p}{k} \quad (1.3)$$

where ρ is the fluid density, g is the gravitational acceleration, C_p is the fluid specific

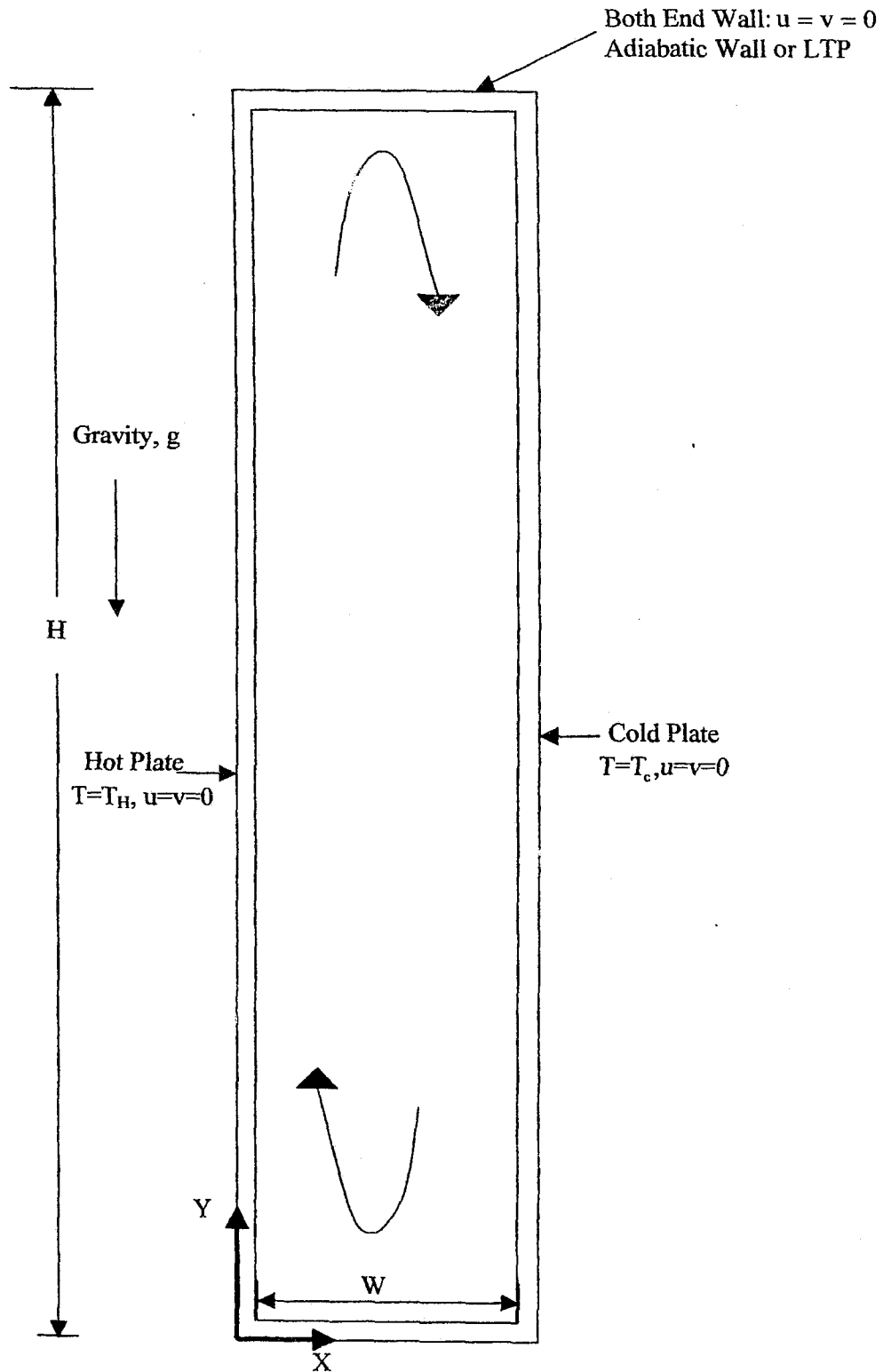


Figure 1.2 Natural convection in tall cavity.

heat, μ is the fluid viscosity, k is the fluid thermal conductivity, H is the height of the cavity, W is the width of the cavity, and β is the coefficient of thermal expansion. Rayleigh number (Ra) is a product of Grashof number (Gr) and Prandtl number (Pr):

$$Ra = GrPr \quad (1.4)$$

In a rectangular cavity, the temperature difference between the vertical walls drives the convective flow. Figure 1.3 shows the variation of average Nusselt number with Rayleigh number for various values of aspect ratio (A). In Figure 1.3 the aspect ratio corresponds to tall cavities with $A \geq 40$. For all aspect ratios, at low Rayleigh numbers, the Nusselt number equals one. At $Nu_{Avg}=1$, the total amount of convective heat transfer is equal to the amount that would exist if the gas were stagnant and transferring energy purely by conduction. This is called the conduction regime. However, the $Nu_{Avg}=1$ condition must not be interpreted as a zero-flow condition. At higher values of Ra the amount of convective flow is greater and Nu increases. The average Nusselt number for tall vertical enclosures can be found in many experimental and numerical studies in the literature (e.g., Elsherbiny et al., 1983; Lee and Korpela, 1983; Wright and Sullivan, 1994).

As shown in Figure 1.4, the critical value of Ra at which the Nusselt number leaves the conduction regime is a function of aspect ratio, A . The convective flow leaves the conduction regime at lower values of Ra for cavities with lower values of A . If the Ra increases sufficiently, instabilities occur that eventually leads to a turbulent boundary layer flow. The critical value of Ra for the onset of turbulent flow is a function of A . The flow in enclosures with larger aspect ratio becomes turbulent at smaller values of Ra .

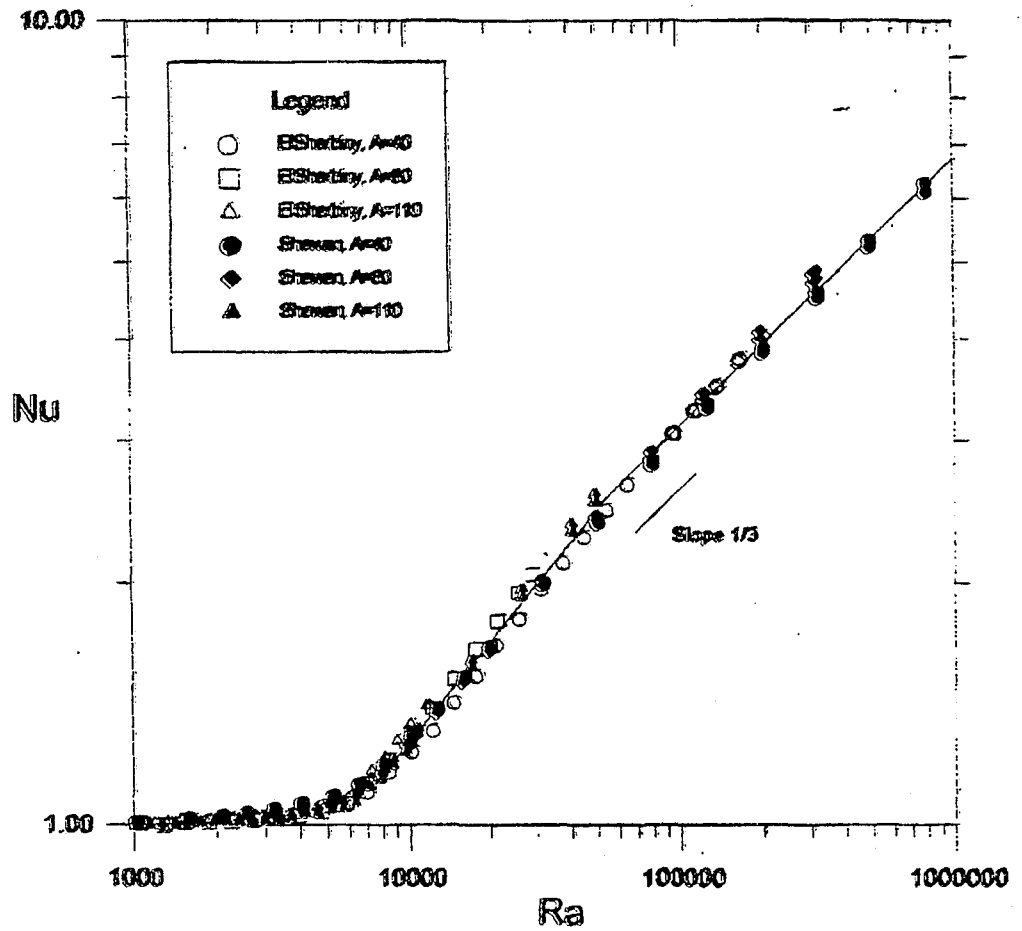


Figure 1.3 Heat transfer measurements by Elsherbiny et al. (1982) and Shewen et al. (1986) for cavities with $A \geq 40$ (Wright, 1996)

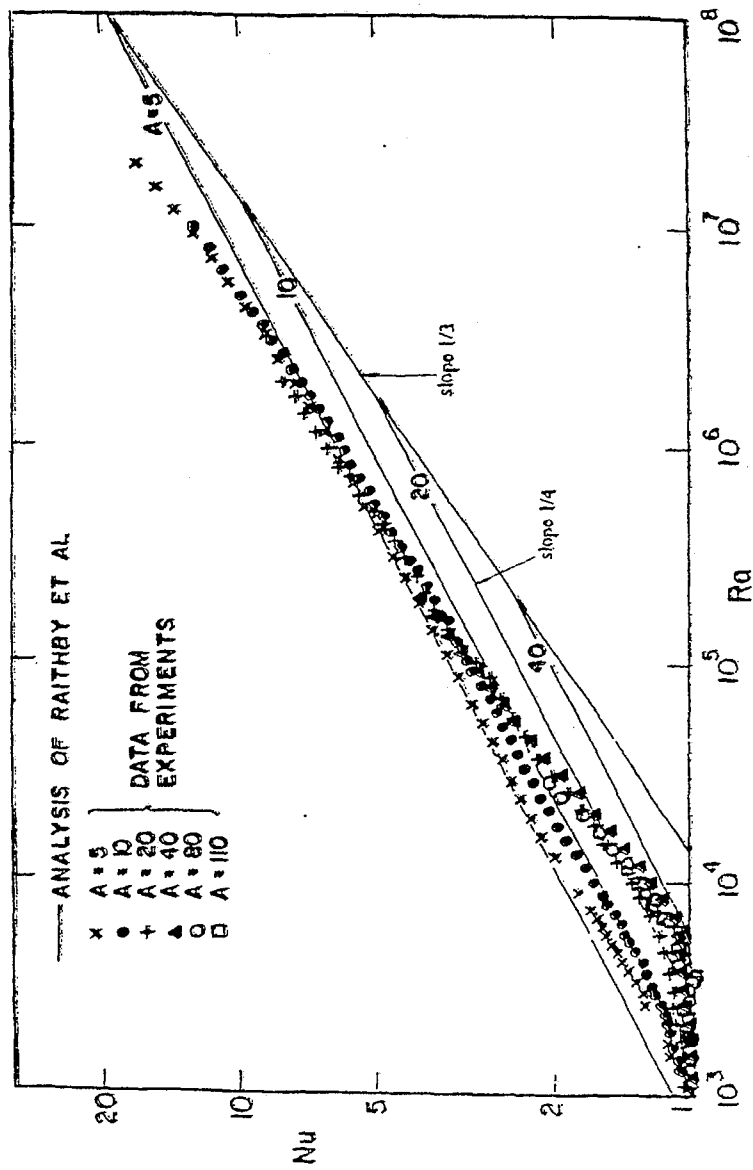


Figure 1.4 A Data of ElSherbiny et al. (1982) and theory of Raithby and Hollands (1982)

At low Rayleigh number, the flow in the cavity is unicellular. When the Rayleigh number reaches a critical value, a steady multicellular flow arises. It was predicted by theoretical analyses (e.g. Vest and Arpaci, 1969; Bergholz, 1978), numerical simulation (e.g. Korpela et al., 1982, 1983), and verified by experiments (e.g. Vest and Arpaci, 1969). The critical value of Rayleigh number Ra_c is given by results of stability analysis (Bergholz, 1978):

$$Ra_c = Gr_c Pr \quad (1.5)$$

where Gr_c is a critical Grashof number and it is defined as:

$$Gr_c = 8 \times 10^3 \left(1 + \frac{5}{A}\right) \quad (1.6)$$

In the current study, many of the calculations are done for $A=20$. For $A=20$, the value of Gr_c is 10^4 . Taking $Pr=0.7$ (air, argon, krypton), the corresponding Ra_c is 7,000.

The data of ElSherbiny et al. (1983) showed that the aspect ratio strongly influenced the heat transfer for low aspect ratio. This data was used to obtain a design correlation. This correlation was developed on the basis of the two sets of Nu/Ra data available for high aspect ratio cavities. The first set was measured by ElSherbiny et al. (1980) and second set was measured by Shewen (1986). Later, Wright (1996) used these data to obtain the following improved correlation:

$$Nu_{Avg} = 0.0673838 Ra^{1/3} \quad Ra > 5 \times 10^4 \quad (1.7)$$

$$Nu_{Avg} = 0.028154 Ra^{0.4134} \quad 10^4 < Ra \leq 5 \times 10^4 \quad (1.8)$$

$$Nu_{Avg} = \left(1 + 1.75966 \times 10^{-10} Ra^{2.2984755}\right) Ra \leq 10^4 \quad (1.9)$$

1.2.2 Studies of the Effect of Blinds on Window Thermal Performance

Several previous experimental and numerical studies have examined the effect of Venetian-type blinds on window thermal performance. A Venetian blind is a shading device that consists of many horizontal louvers, which can be rotated around a horizontal axis. Some studies have considered the effect of a Venetian blind located adjacent to the indoor glazing surface. Others have considered the effect of an inter-pane Venetian blind. A brief review of the literature in this area will be presented in this section.

Machin et al. (1997) has performed an experimental study on the effect of louvers adjacent to an isothermal flat surface, which approximated a window glazing. Local convection coefficients were obtained using laser interferometry at three different blind spacings and four different blind angles. Except at very close spacing, the effect of the blind on the average convective heat transfer rate was found to be less than 13%, compared to an isolated flat plate.

Phillips (1998) has obtained a numerical solution for the effects of blinds on the convective and radiative heat transfer rates from an isothermal window glazing surface for three different blind angles and spacings. In this study, Phillips reported that the presence of the louvered blind results in periodic variation in the local convective and radiative heat transfer rate. In this study, Phillips (1998) reported that the blind provides shielding that reduces the radiative heat transfer rates from the window by up to 38% compared to an unshaded window.

Garnet et al. (1999) has measured the center-glass U-Value of a window with an inter-pane Venetian blind for several different blind louver angles. These experimental measurements were made using a guarded heater plate apparatus. Garnet (2000) also

developed a finite-volume CFD model of his experiment. However, convergence problems occurred and only a limited set of results were obtained.

Shahid (2001) did a numerical study on convective heat transfer rate from an isothermal vertical surface adjacent to a set of horizontal louvers using the finite element code FIDAP. Shahid used the CFD results in a simplified one-dimensional model of the complete fenestration system to determine key performance indicators (e.g., U-Value). The results showed that Venetian blinds could have a significant beneficial effect on the window thermal performance. For a double glazed window the U-value decreased by as much as 20%.

Yahoda and Wright (2004) have presented a simple one-dimensional model for predicting the thermal resistance of a double glazed window with a between panes louvered blind. They used empirical correlations for a simple vertical enclosure to estimate the convective heat transfer coefficients. Despite this crude approximation, the predicted U-Values were within 10% to 15 % of the experimental U-Values measured by Garnet (1999).

Naylor and Collins (2004) have extended the work of Yahoda and Wright (2004). Naylor and Collins (2004) used a conjugate convection-conduction CFD model to predict the convective heat transfer coefficients in a window with an inter-pane Venetian blind. These heat transfer coefficients were then used with a simplified radiation model to predict the U-Value of the window/blind system. They concluded from their study that this approach can be used to predict the overall heat transfer rate with high accuracy.

Recently, Lai (2004) has done an experimental study to measure the free convective heat transfer in a double-glazed window with a between-panes Venetian blind.

Experiments were conducted using a Mach-Zehnder interferometer for three slat angles and for three cavity widths. This study provided temperature field visualization as well as detailed local Nusselt number data on the hot and cold glazings.

All of the previous studies have been done for a Venetian-type blind. To the author's knowledge, there are no comparable studies for a pleated blind. In the present study, a two-dimensional CFD model is developed to study the heat transfer in a window with a between-panes pleated blind.

1.3 Problem Geometry

Figure 1.1(b) shows a window with a between-panes pleated blind manufactured by Pella, which is currently available on the market. The detailed problem geometry is illustrated in Figure 1.5. Measurements were taken from Pella's recently launched product. The thickness of blind was measured to be $t=0.20\text{mm}$ and the width of the blind was measured to be $S=16\text{mm}$. In the current study, this blind was placed into an enclosure with a width of $W=25\text{mm}$. The aspect ratio was taken to be $A=20$ and $A=40$ for the present study.

It should be noted that $A=20$ and $A=40$ are nominal values, since it was chosen to have an integer number of blind pleats i.e., it was necessary to adjust the enclosure height slightly in order to avoid a partial pleat. It will be shown later in the results that the enclosure aspect ratio has a very weak effect on the average Nusselt number. So, the effect of this small height adjustment is expected to be small.

The model geometry shown in Figure 1.5 has height H and width W . T_H and T_C are respectively hot side and cold side glazing temperatures of the enclosures, T_B is the

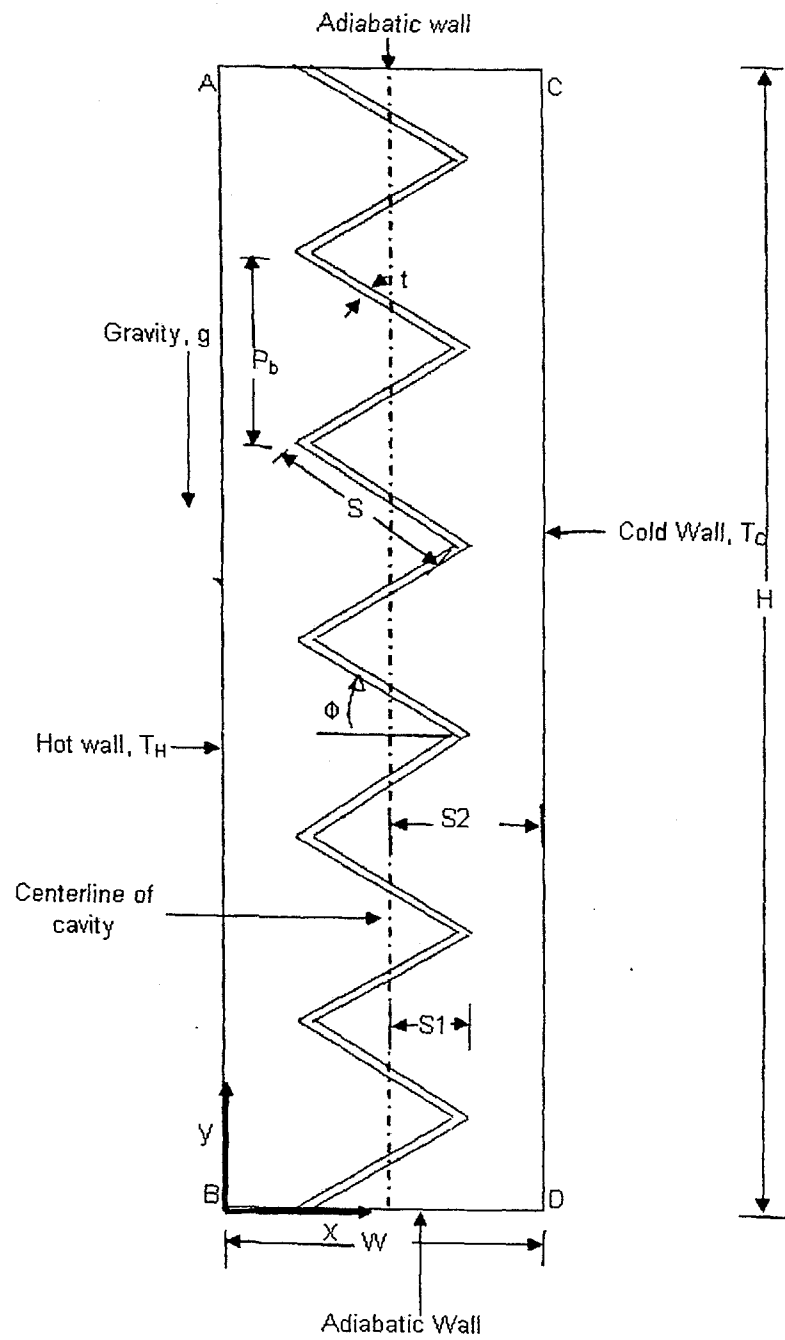


Figure 1.5 Geometry of pleated blind inside a double glazed window.

blind temperature, k_B is the conductivity of blind and Φ is an angle between blind. The blind is kept in the center for all the results that are presented in the coming chapter. In the present study, cotton is taken as the blind material ($k_B=0.059\text{W/mk}$). The blind pitch (P_b) in the present case varies as the angle changes. P_b , t and S are the pitch, thickness and width of the blind respectively. S_1 is a projection length of a blind from the extreme edge to the center and S_2 is the half cavity width. The blind emissivity ϵ_B is kept constant ($\epsilon_B=0.8$). ϵ_H and ϵ_C are respectively the hot side and cold side glazing surface emissivities.

1.4 Objective of Present Study

The objective of this project is to gain an understanding of how a pleated blind inside a vertically oriented double glazed window will influence the free convection between the panes of the window. In the present study, a two-dimensional CFD model is developed to study the conjugate conduction/convection heat transfer effects in a window with a between-panes pleated blind. This study examines the effect of various geometric parameters for both the cavity and the blind on the window thermal performance.

It is then shown that these CFD results (without radiation effects) can be combined with a simple radiation model to obtain the conjugate conduction, convection and radiation heat transfer through the window/blind system.

2.1 Introduction

In order to obtain a numerical solution, the physical problem must be described in mathematical terms. This involves defining governing equations that apply over the relevant computational domain and then implementing boundary conditions.

The preprocessing tool GAMBIT is used for the meshing window blind system and FLUENT 6.0 is used for the CFD calculation. The geometry of the window and blind is shown in Figure 1.5. The issues of grid dependency and validation of the results are also addressed. A grid sensitivity study is performed and the numerical solution is validated by comparing with De Vahl Davis and Jones (1983) bench mark solution.

In the present work, heat transfer effects are studied in the cavity between the hot and cold glazing surfaces. In this model, the Nusselt number is calculated for a range of Rayleigh numbers to determine an effect of the pleated blinds on the thermal energy performance. It has been calculated that the practical range of Rayleigh numbers for the current problem is approximately $10^3 \leq Ra \leq 10^5$. For the current geometry, the upper limit ($Ra = 10^5$) occurs for ASHRAE (2001) winter design conditions. These temperature conditions ($T_C = -18^\circ\text{C}$, $T_H = 21^\circ\text{C}$) correspond to a larger temperature difference than for ASHRAE summer design conditions.

For the current study, the average Nusselt number is a function of:

$$Nu_{Avg} = f(Ra, Pr, A, k_F/k_B, \text{blind geometry}) \quad (2.1)$$

The Nusselt number is defined by the following equation:

$$\text{Nu}_{\text{AVG}} = \frac{Q_{\text{CONV}} W}{(T_{\text{H}} - T_{\text{C}}) k_{\text{F}} H} \quad (2.2)$$

where Q_{CONV} is the average convective heat transfer rate, W is width of cavity and k_{F} is the thermal conductivity of filled gas. Most of the numerical results in following sections are presented for air.

2.2 Governing Equations

Free convection motion of the fluid occurs due to density changes arising from the heating process. The buoyancy forces which give rise to the free convection currents are called body forces. In the present study, the body force is gravitational, and the density gradients are due to temperature variations within the flow field. To describe natural convective heat transfer, the continuity, momentum and energy equations are required. These equations result from applying the laws of conservation of mass, momentum and energy to a control volume. In general, these conservation principles represent mathematical models of the behavior of the physical problem and they are adequate for the analysis of the vast majority of engineering problems. These conservation principles lead to the so-called continuity, Navier-Stokes and energy equations.

Equations (2.3) through (2.6) are the continuity, x and y momentum equations, and the energy equation for the flow field (Oosthuizen and Naylor (1999)). The flow is assumed to be steady, laminar, incompressible and two-dimensional. The thermo physical properties of fluid and solid are assumed to be constant, except for fluid density which is treated by means of the Boussinesq approximation.

$$\frac{\partial u}{\partial x} + \frac{\partial v}{\partial y} = 0 \quad (2.3)$$

$$\rho \left(u \frac{\partial u}{\partial x} + v \frac{\partial u}{\partial y} \right) = - \frac{\partial p}{\partial x} + \mu \left(\frac{\partial^2 u}{\partial x^2} + \frac{\partial^2 u}{\partial y^2} \right) \quad (2.4)$$

$$\rho \left(u \frac{\partial v}{\partial x} + v \frac{\partial v}{\partial y} \right) = - \frac{\partial p}{\partial y} + \mu \left(\frac{\partial^2 v}{\partial x^2} + \frac{\partial^2 v}{\partial y^2} \right) - \rho g \quad (2.5)$$

$$u \frac{\partial T}{\partial x} + v \frac{\partial T}{\partial y} = \alpha \left(\frac{\partial^2 T}{\partial x^2} + \frac{\partial^2 T}{\partial y^2} \right) \quad (2.6)$$

The last term of eq. (2.5) represents the body force acting through the fluid medium which produces the buoyancy induced fluid motion in the vertical direction. By assuming a constant fluid density, the body force term in eq. (2.5) has become a constant. The Boussinesq approximation must be implemented in eq. (2.5) so that the temperature induced fluid density variations may be re-introduced into the body force term. It should be noted that the Boussinesq approximation will account for fluid density variations in the body force term only. This is accomplished by first defining a pressure defect between an arbitrary location within the flow field and the ambient pressure:

$$p' = p - p_{\infty} \quad (2.7)$$

The ambient pressure is simply the hydrostatic pressure measured from some reference datum, so that:

$$p_{\infty} = -\rho_{\infty} g y \quad (2.8)$$

Now note the change in the pressure difference p' in the x and y directions respectively:

$$\frac{\partial p'}{\partial x} = \frac{\partial p}{\partial x} \quad (2.9)$$

$$\frac{\partial p'}{\partial y} = \frac{\partial p}{\partial y} + \rho_{\infty} g \quad (2.10)$$

In the case of an incompressible flow, the influence of the temperature changes on density changes is significant and the influence of pressure changes on density changes is negligible. Therefore, it is convenient to express the buoyancy force in terms of the temperature difference. This can be achieved by introducing the temperature coefficient of the bulk expansion β , such that

$$(\rho_{\infty} - \rho)g \approx \rho g \beta (T - T_{\infty}) \quad (2.11)$$

Substituting eqs. (2.9) to (2.11) gives:

$$\rho \left(u \frac{\partial u}{\partial x} + v \frac{\partial u}{\partial y} \right) = -\frac{\partial p'}{\partial x} + \mu \left(\frac{\partial^2 u}{\partial x^2} + \frac{\partial^2 u}{\partial y^2} \right) \quad (2.12)$$

$$\rho \left(u \frac{\partial v}{\partial x} + v \frac{\partial v}{\partial y} \right) = -\frac{\partial p'}{\partial y} + \mu \left(\frac{\partial^2 v}{\partial x^2} + \frac{\partial^2 v}{\partial y^2} \right) + g \rho_{\infty} \beta (T - T_{\infty}) \quad (2.13)$$

Conduction through the pleated blind is an important factor in the heat exchange across the window. Steady conduction through blind is governed by Laplace's equation:

$$\frac{\partial^2 T}{\partial x^2} + \frac{\partial^2 T}{\partial y^2} = 0 \quad (2.14)$$

At the blind-fluid interfaces, no slip and impermeability conditions are applied. In addition to a continuity of temperature, continuity of heat flux is also applied at these interfaces, expressed as follows:

$$-k_B \frac{\partial T}{\partial n} \Big|_{\text{blind interface}} = -k_F \frac{\partial T}{\partial n} \Big|_{\text{fluid interface}} \quad (2.15)$$

where n is the normal vector to the surface, k_B and k_F are the blind and fluid conductivities. Air was the fill gas in most of the cases. The governing equation have been solved using the CFD software FLUENT.

2.3 Boundary Conditions

Listed below are the boundary conditions in dimensional form for the computational domain depicted in Figure 1.5. To solve the continuity, momentum and energy equations the following boundary conditions were applied:

$$u = v = 0, T = T_H \quad \text{for } x=0, \quad 0 \leq y \leq H \quad (\text{AB})$$

$$u = v = 0, T = T_c \quad \text{for } x=W, \quad 0 \leq y \leq W \quad (\text{CD})$$

$$u = v = \frac{\partial T}{\partial y} = 0 \quad \text{for } y=0, H \quad 0 \leq x \leq W \quad (\text{AC, BD})$$

In Fig 1.5 boundaries AB, CD, AC and BD represent solid boundaries where no slip and impermeability boundary conditions apply. The temperatures along boundary AB and CD were set to constant value to model the isothermal centre-of-glass region. In Figure 1.5, boundaries AC and BD represent the adiabatic end walls.

2.4 Properties of Different Fill Gases and ASHRAE Design Conditions

The maximum Rayleigh number studied corresponds to the temperature difference between the window glazings for ASHRAE winter design conditions (ASHRAE Fundamentals Handbook, 1993). The ASHRAE winter and summer design conditions are shown below in Table 2.1.

The properties of various fill gases (air, argon, krypton) have been calculated using the correlation equations given in the VISION reference manual:

Table 2.1 ASHRAE design conditions for summer and winter

	Indoors Temp (°C)	Outdoors Temp (°C)	Cloud Cover (%)	Wind Speed V_0 (m/s)
Summer	24	32	100	3.35
Winter	21	-18	100	6.7

Air

$$k = (0.095328 + 0.0033086T_m) 2.414 \times 10^{-2}, \text{ W/mK}$$

$$\mu = (0.0035165 + 0.0000498T_m), \text{ g/ms}$$

$$C_p = (2.525325 - 0.0000661T_m) 8.3152, \text{ J/gmoleK}$$

Argon

$$k = (0.151607 + 0.0031036T_m) 1.634 \times 10^{-2}, \text{ W/mK}$$

$$\mu = 0.003618 + 0.0000644T_m, \text{ g/ms}$$

$$C_p = (2.525325 - 0.0000661T_m) 0.208152 \times 39.948, \text{ J/gmoleK}$$

Krypton

$$k = (0.855136 + 0.0286275T_m) 1.0 \times 10^{-3}, \text{ W/mK}$$

$$\mu = 0.00234 + 0.0000783 T_m, \text{ g/ms}$$

$$C_p = 0.2497 \times 83.8, \text{ J/gmoleK}$$

where T_m is the mean gas layer temperature in Kelvin. All of the results presented in Chapter 3 are based on these correlations.

2.5 Grid Sensitivity for Convection Numerical Model

A detailed grid sensitivity study has been conducted on the computational domain to ensure that the numerical solutions were independent of the grid density. To ensure

grid density independence, the number of nodes within the computational domain was increased by 2.7 times. Figure 2.1 shows the grids for three cases. Table 2.2 and Figure 2.2 show the comparison of these three cases. The number of nodes in case 1, case 2 and case 3 are 39935, 76255 and 106893, respectively. Over the full range of Rayleigh number, the average Nusselt numbers listed in Table 2.2 differ by only 0.5 %, even though the number of nodes was increased by approximately 2.7 times. Furthermore, increasing the number of nodes within the computational domain greatly increases the time required for the solution process. It was found that solutions on the fine grid took almost five times longer than solutions on the coarse grid. Based on these results, the numerical calculations in this thesis were done using a grid density comparable to Case 1. The low grid density was used in order to reduce the computational time for solution procedure. A XEON™ 3.0 GHz processor was used for the numerical study. The following convergence criteria were used: 10^{-3} for continuity, x-momentum and y-momentum, and 10^{-6} for energy.

Table 2.2 Grid independency study for case 1, case 2, and case 3 for $10^3 \leq Ra \leq 10^5$ ($A=20$, $Pr=0.71$, $\Phi=60^\circ$, $k_B/k_F=2.53$)

Ra	Nu _{AVG}		
	Case 1=39935 Nodes	Case 2= 76255 Nodes	Case 3= 106893 Nodes
1000	1.005	1.005	1.006
2000	1.009	1.009	1.009
4000	1.024	1.024	1.024
6000	1.046	1.045	1.045
10000	1.099	1.100	1.097
20000	1.224	1.226	1.222
40000	1.383	1.385	1.380
60000	1.477	1.477	1.472
100000	1.602	1.601	1.594

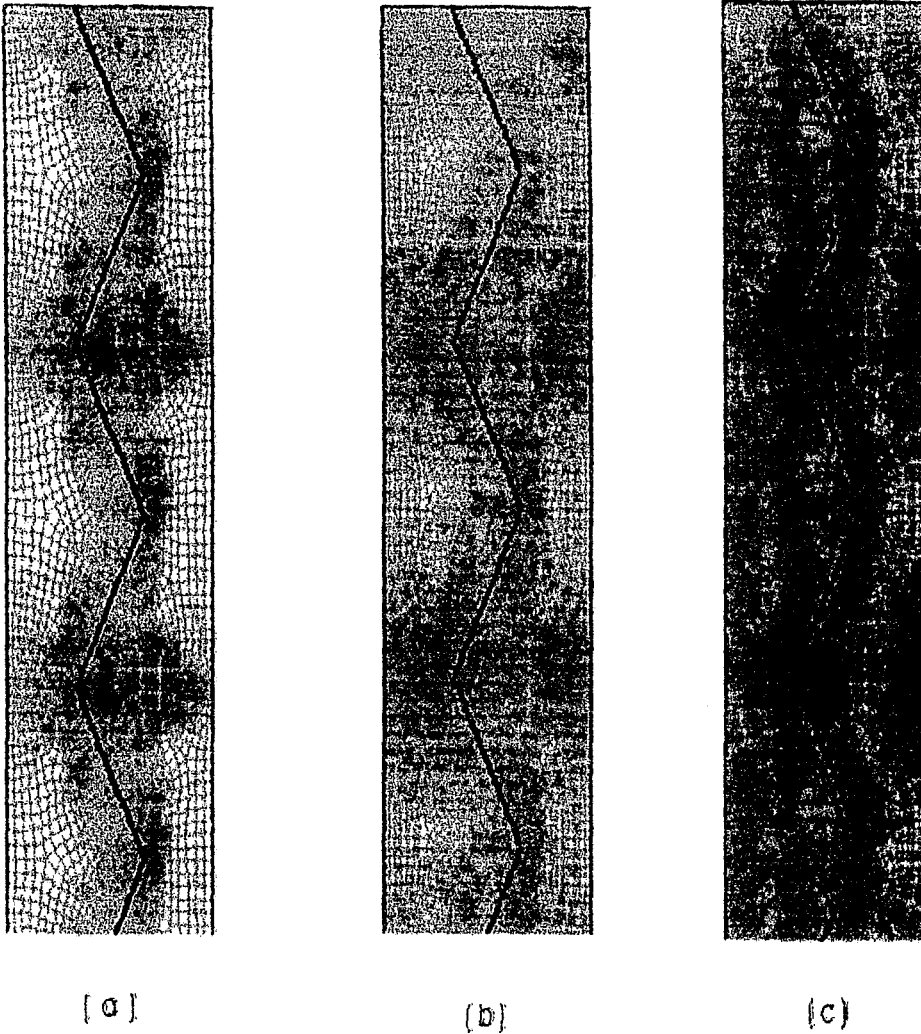


Figure 2.1 Three different grid densities at $\Phi=60^{\circ}$ for (a) Case 1:39935 Nodes (b) Case 2:76255 Nodes (c) Case 3:106893 Nodes.

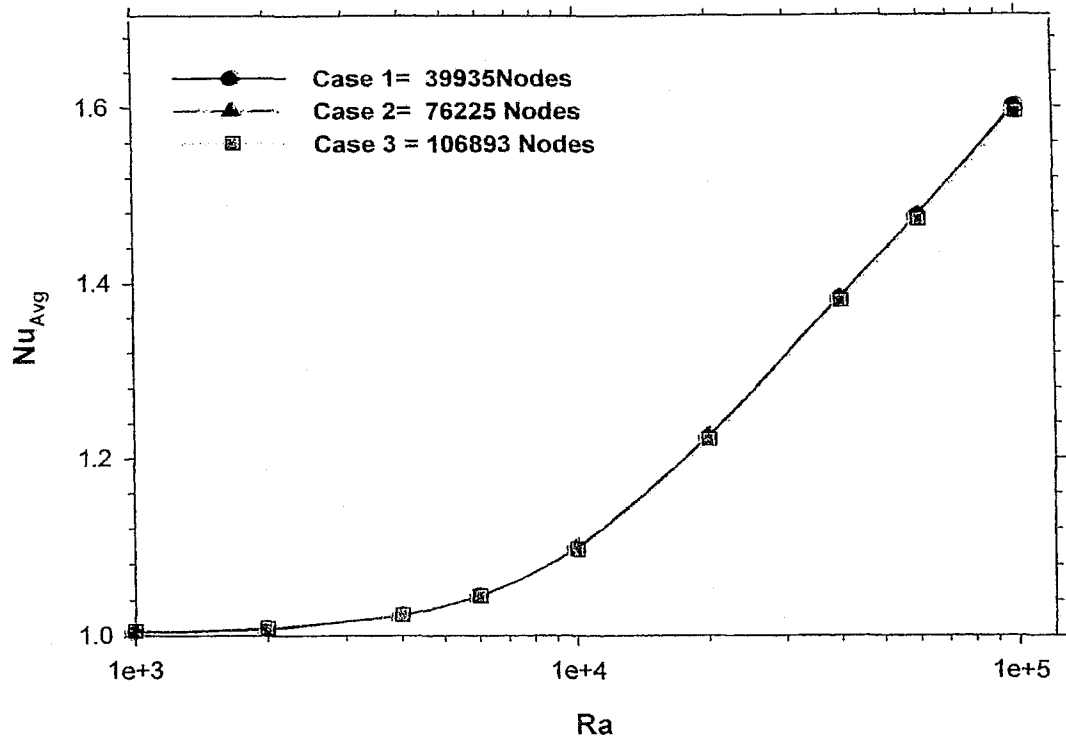


Figure 2.2 Comparison of the three meshes used for the grid sensitivity study ($A=20$, $\Phi=60^\circ$, $Pr=0.7$, $k_B/k_F=2.53$).

2.5.1 Solution validation with the bench mark solution of De Vahl Davis and Jones (1983) for a square enclosure

Numerical studies require careful validation of the code and model being used. In this study, the commercial CFD software FLUENT 6.0 has been used, which is a finite volume code. To check the functionality of the commercial software package being used for this study, a numerical solution has been compared to the benchmark solution of De Vahl Davis and Jones (1983). This benchmark solution is for two-dimensional free convection in a square enclosure ($A=1$). This solution also served to test the grid

generation software (GAMBIT) and the implementation of the boundary conditions and fluid properties within FLUENT. The average Nusselt number has been found for the following range of parameters:

- ❖ $10^3 \leq Ra \leq 10^5$
- ❖ $Pr=0.7$ (nominal value for air, argon, krypton)
- ❖ $A = \frac{H}{W} = 1$

The numerical results shown in Figure 2.3 indicate that, at the highest Rayleigh number $Ra=10^5$ (worst case), the average Nusselt number differs by 2% compared to the De Vahl Davis and Jones (1983) benchmark solution. Figure 2.3 indicates that the numerical code predicts an average Nusselt number very comparable to bench mark solution of De Vahl Davis and Jones (1983) over the entire range of Rayleigh numbers.

2.5.2 Natural convection in 2D rectangular cavity for high aspect ratio ($A = 40$)

The convective flow patterns between a hot plate and cold plate in a 2D rectangular cavity have been studied. The value of average Nusselt number calculated by CFD calculation has been compared with the correlation by Wright (1996). According to the literature, the critical value of Ra at which the Nusselt number leaves the conduction regime is function of A . As shown in Figure 1.3, the average Nusselt number leaves the conduction regime at lower values of Ra in cavities with lower values of A .

Figure 2.4 shows a comparison between the current CFD study and the correlation by Wright (1996). It can be seen in this Figure that the CFD results and correlation results are within 5% at low Rayleigh numbers. At high Rayleigh numbers, the agreement is closer (about 1.3%).

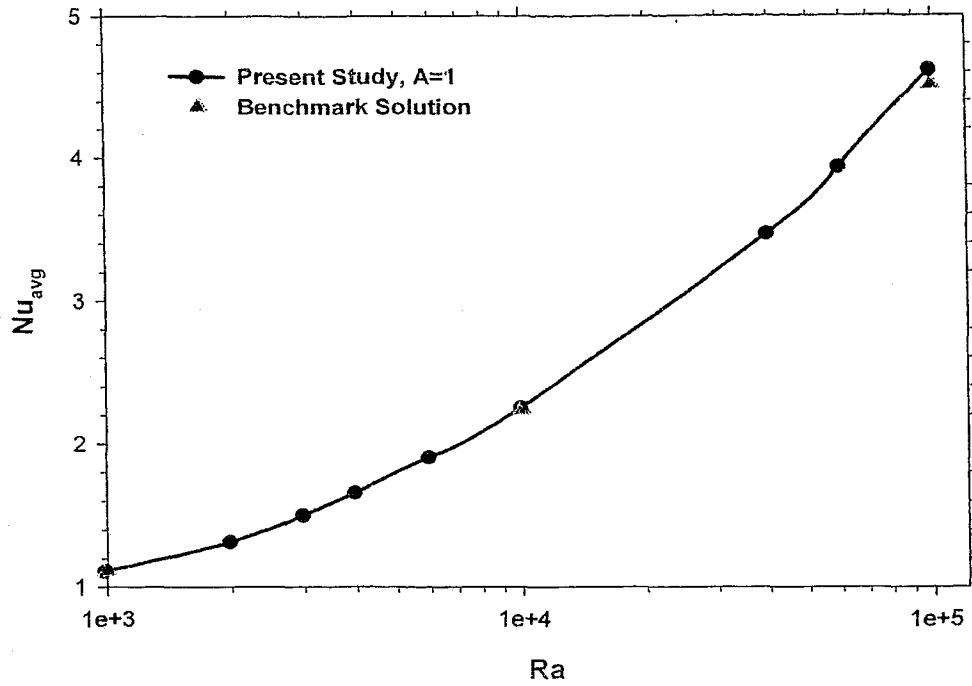


Figure 2.3 Comparison of bench mark solution of De Vahl Davis and Jones (1983) with the current CFD results for $A = 1$.

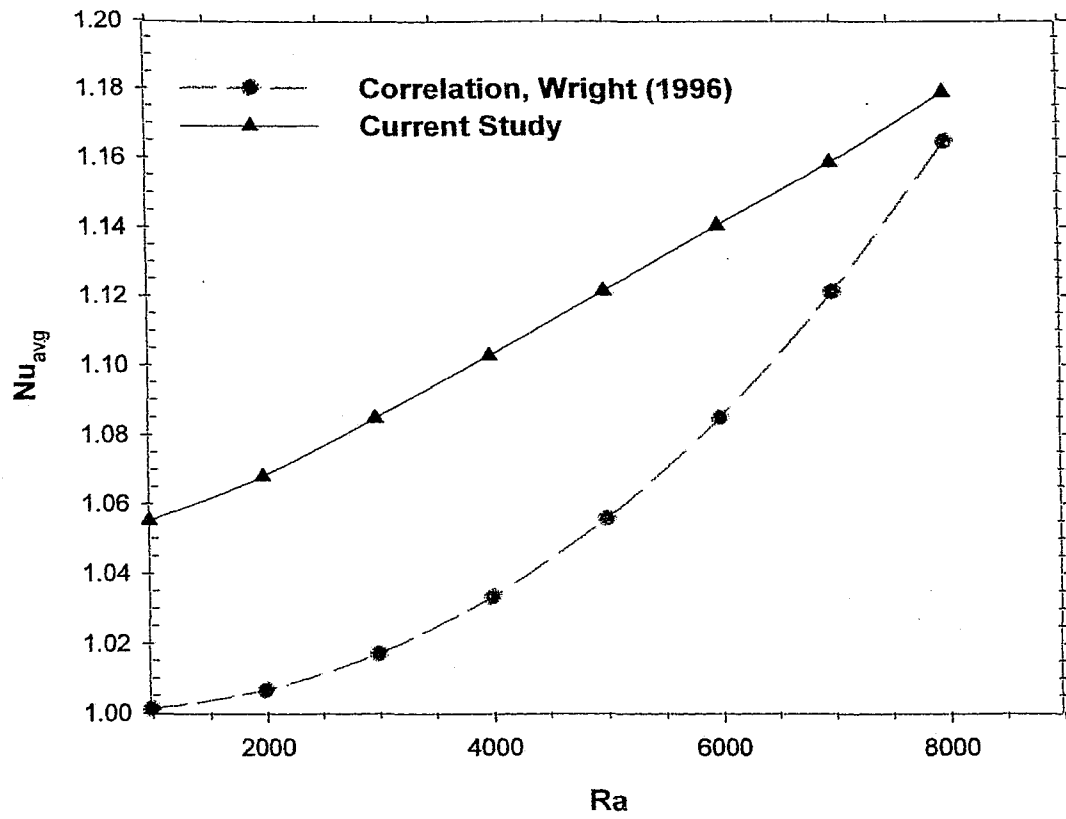


Figure 2.4 Comparison of present numerical calculation for $A=40$ with the correlation of Wright (1996) ($Pr=0.7$).

CHAPTER 3: PRESENTATION OF RESULTS

3.1 Introduction

In this chapter, selected numerical results are presented and the effects of a pleated blind on the energy performance are shown. The effect of Rayleigh numbers on the average Nusselt number is compared for different blind geometries in Section 3.2. In the last section of this Chapter, a comparison is made between a two-dimensional CFD model which includes radiation effects, and a simplified one-dimensional model.

A sample of input file for the mesh generation is given in Appendix A. Also, selected numerical results from this study are presented in tabular form in Appendix B.

3.2 Results from the Free Convection CFD Model

Finite volume solutions were obtained for different blind geometries to compute the convective heat transfer between the panes of the double glazed window. The range of Rayleigh numbers has been taken to be $10^3 \leq Ra \leq 10^5$ and the fluid Prandtl number was taken to be $Pr=0.71$. This Prandtl number corresponds (approximately) to that of air, krypton and argon, in the temperature range of typical window applications. The aspect ratio was taken to be $A=20$ and $A=40$ for most of the cases and blind width was taken to be $S=16\text{mm}$. The enclosure width was taken to be $W=25\text{mm}$.

Temperature difference between hot and cold glazings was fixed at $\Delta T=1^\circ\text{C}$. Although the Rayleigh number could have been adjusted by changing the temperature difference between the glazings, in the current study the Rayleigh number was increased by increasing gravity (g). This approach was taken to allow converged solutions at lower Rayleigh numbers to be used as the initial value for next the iterative solution at higher

Rayleigh number. This is called “incremental loading” and improves the likelihood of achieving convergence, particularly at high Rayleigh number.

3.2.1 Effects of Properties of Selected Gases on the Convective Heat Transfer

In this section, results are compared for three different filled gases (air, argon and krypton) that are commonly used in insulated glazing units. The properties of air, argon and krypton are calculated using the equations from the VISION reference manual, which are given in previous chapter. It should be noted that the Prandtl number for air, argon and krypton are approximately the same ($Pr \approx 0.71$).

Figure 3.1 shows the variation of the average Nusselt number with Rayleigh number for the three different fill gases. It can be seen that the fill gas has only a slight effect on the average Nusselt number over the full range of Rayleigh number. This result is expected, since the Prandtl numbers are approximately same. The slight difference in the results for the three gases is caused by the slight difference in the conductivity ratio. In these three cases, the blind to gas thermal conductivity ratio (k_B/k_F) varies from 2.35 (for air) to 6.25 (for krypton).

3.2.2 Effects of Blind thermal Conductivity on the Convective Heat Transfer

There are various types of blind material available on the market. For pleated blinds, the material may be paper, cotton, silk or fiber. Table 3.1 shows the range of thermal conductivities for various materials that might be used.

Figure 3.2 shows the effect of blind conductivity on the average Nusselt number. It is interesting to note that the blind conductivity ratio has a strong effect on the average

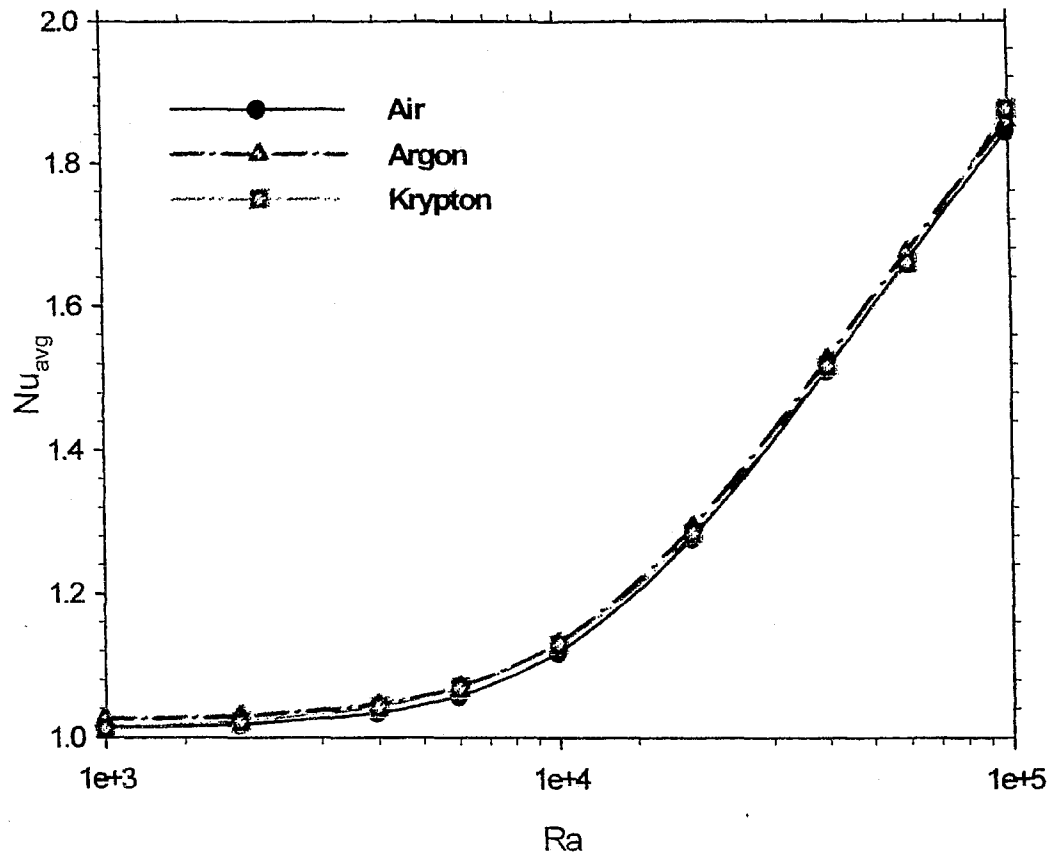


Figure 3.1 Effect of Rayleigh number on average Nusselt number for different fill gases ($A=20$, $\Phi=45^\circ$, $S1/S2=0.4525$).

Nusselt number over the range of Rayleigh number $10^3 < Ra < 10^5$.

It can be seen in Figure 3.2 that the blind thermal conductivity has the greatest effect at low Rayleigh numbers. The average Nusselt number for $k_B/k_F=42.9$ is 15.6% higher than that for $k_B/k_F=2.53$, in the conduction regime. However, as the convection strengthens at higher Rayleigh numbers, the difference in the average Nusselt numbers decreases. At $Ra=10^5$, the average Nusselt numbers differs by only 3.5%. The effect of blind conductivity is less at high Ra because convection plays a more dominant role in the overall heat transfer.

Table 3.1 Conductivity of different materials suitable for a pleated blind.

Blind material	W/mK	k_B/k_F^*
Paper	0.059	2.24
Felt	0.036	1.37
Linen	0.088	3.35
Silk	0.04	1.52
Cotton	0.059	2.53
PVC	0.19	7.22
PTFE	0.25	9.51

*Conductivity ratio for air as the fill gas.

3.2.3 Effects of Blind Width on Convective Heat Transfer

It is interesting to find the effect of blind width (S) on heat transfer rate. Figure 3.3 shows the effect of blind width on the average Nusselt number for a range of Rayleigh numbers. Three cases are considered: $S=14\text{mm}$, $S=16\text{mm}$ and $S=18\text{mm}$. The ratio $S1/S2$ (see Figure 1.5) indicates the proximity of the blind tips (i.e., the folds) to the window glazings. The corresponding stream function contours and temperature contours

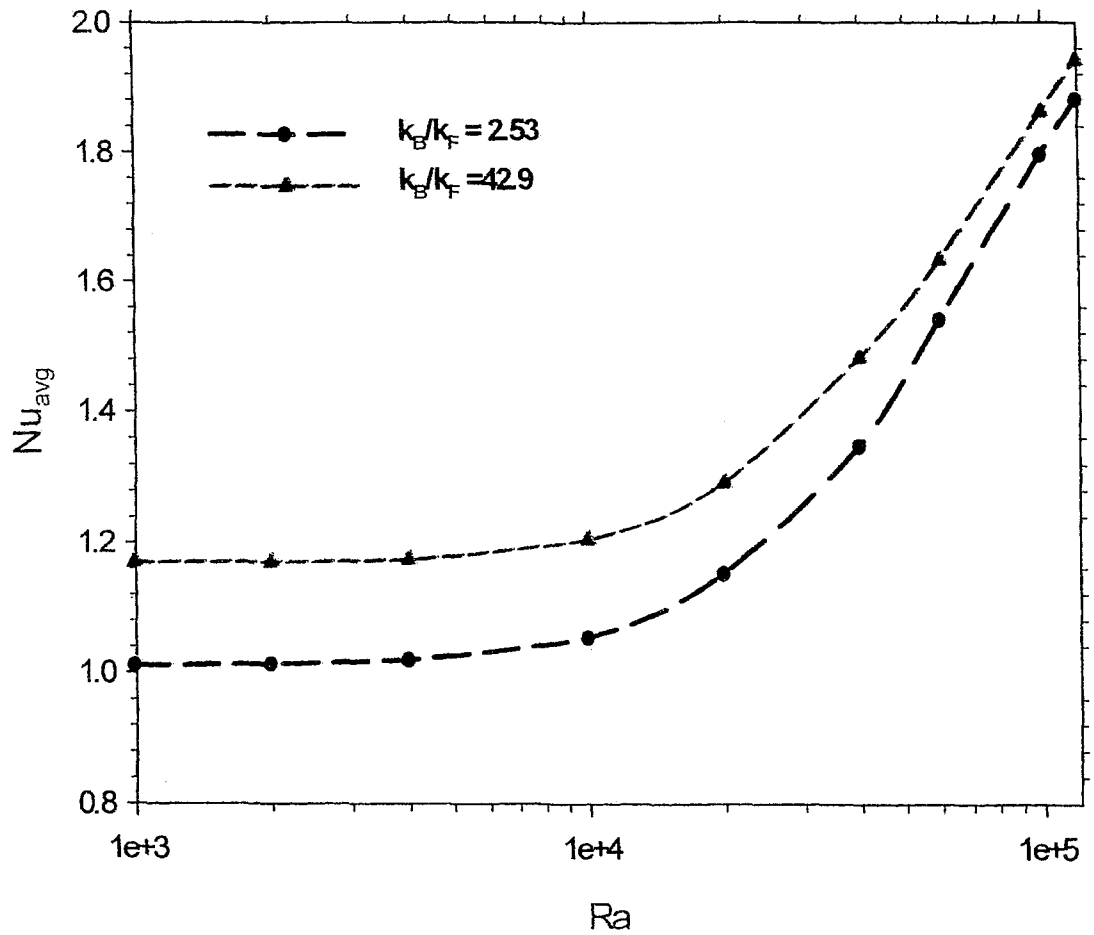


Figure 3.2 Effect of Rayleigh numbers on average Nusselt number for different blind conductivity ($Pr=0.71$, $A=20$, $\Phi=45^\circ$).

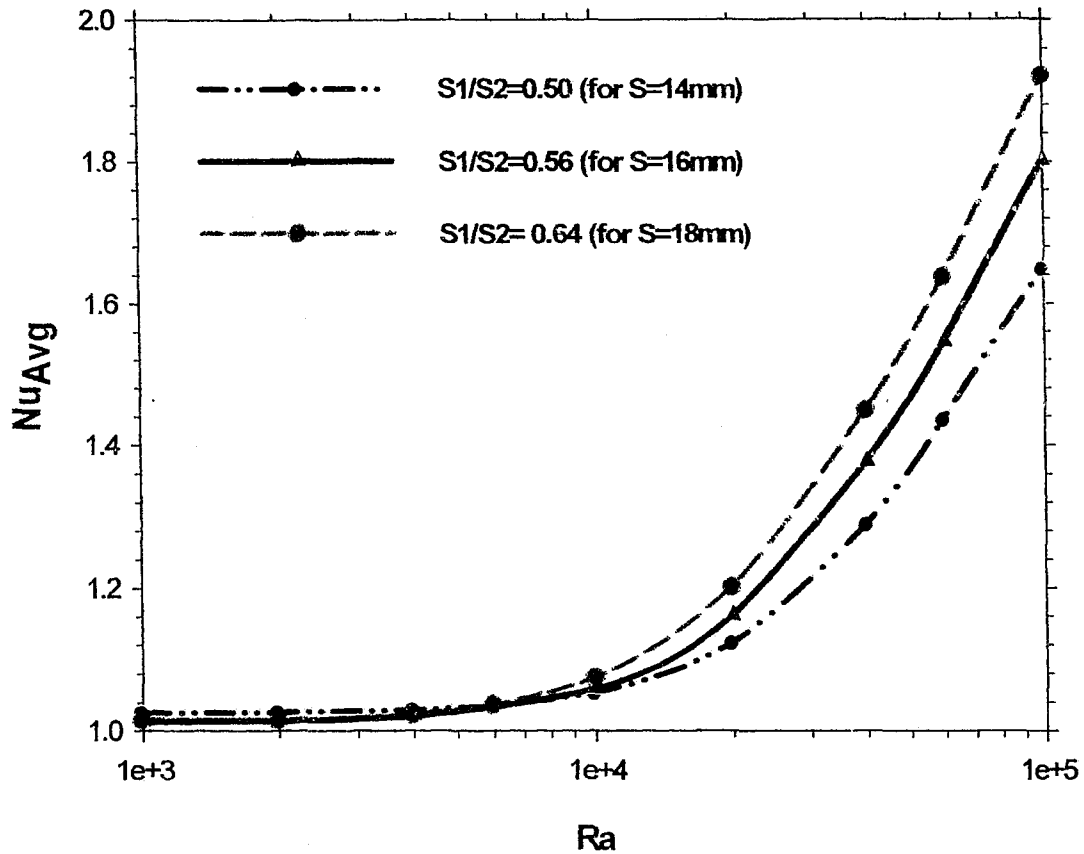


Figure 3.3 Effect of Rayleigh number on the average Nusselt number for different blind widths ($A=20$, $\Phi=30^\circ$, $Pr=0.71$, $k_B/k_F=2.53$).

for these three cases are shown in Figures 3.4 and 3.5. In the present case, the blind is kept in the center of the enclosure and the blind angle (Φ) is constant at 30° . So, increasing the blind width decreases the gap between tips of blind and the window glazing. It is shown in Figure 3.3 that in the conduction regime (low Rayleigh number), the convective heat transfer is almost unaffected by the blind width. At higher Rayleigh numbers, as convection strengthens, the width of the blind has a stronger effect. As the blind width increases, the average Nusselt number increases. There appears to be two reasons. It can be seen from the stream function contours (Figure 3.4) that the value of the maximum stream function increases as the blind width increases. This indicates that there is a stronger flow on both sides of the blind as S increases. This will tend to increase the convective heat transfer rate. In addition, as mentioned above, increasing S decreases the gap between tips of blind and the window glazing. So, for example, this allows the fluid on the hot side of the enclosure to flow in closer proximity to the cold glazing. This geometric effect also reduces the convective resistance of the enclosure.

3.2.4 Effects of Blind Angle on Convective Heat Transfer

In the present study, the effect of blind angle (Φ) on the heat transfer rate has been examined. Figure 3.6 shows the effect of blind angle on the average Nusselt number for a range of Rayleigh number. Three cases are considered: $\Phi=30^\circ$, $\Phi=45^\circ$ and $\Phi=60^\circ$. The corresponding stream function contours and temperature contours for these three cases are shown in Figures 3.7 and 3.8. It is shown in Figure 3.6, that at low Rayleigh numbers

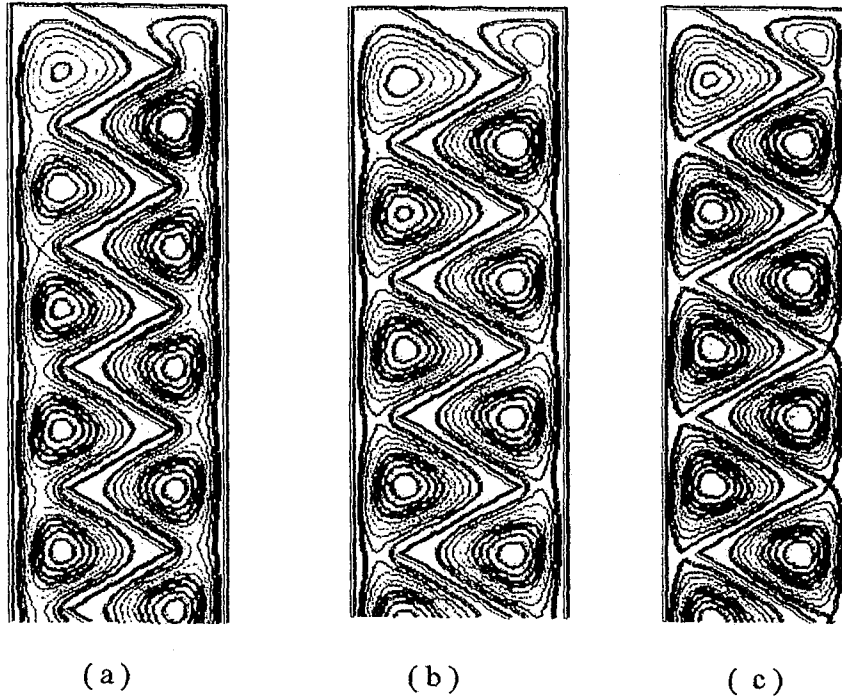
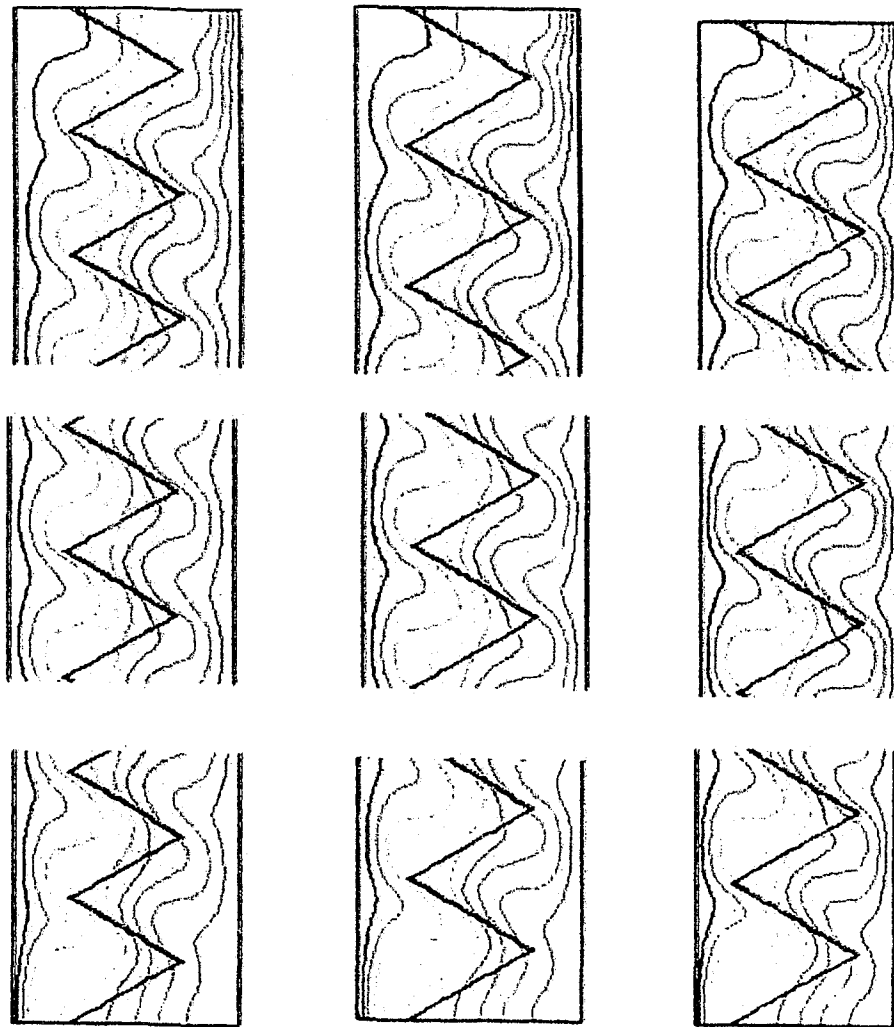


Figure 3.4 Stream function contour for different blind width (a) $S=14\text{mm}$ ($\Psi_{\text{max}}=1.26 \times 10^{-4} \text{m}^2/\text{s}$) (b) $S=16\text{mm}$ ($\Psi_{\text{max}}=1.33 \times 10^{-4} \text{m}^2/\text{s}$) (c) $S=18\text{mm}$ ($\Psi_{\text{max}}=1.36 \times 10^{-4} \text{m}^2/\text{s}$) ($Ra=1 \times 10^5$, $A=20$, $\Phi=30^\circ$, $Pr=0.71$, $k_B/k_F=2.53$).



(a)

(b)

(c)

Figure 3.5 Isotherm contours for the blind width (a) $S=14\text{mm}$ (b) $S=16\text{mm}$ (c) $S=18\text{mm}$ ($Ra=1 \times 10^5$, $A=20$, $\Phi=30^\circ$, $Pr=0.71$, $k_B/k_F=2.53$).

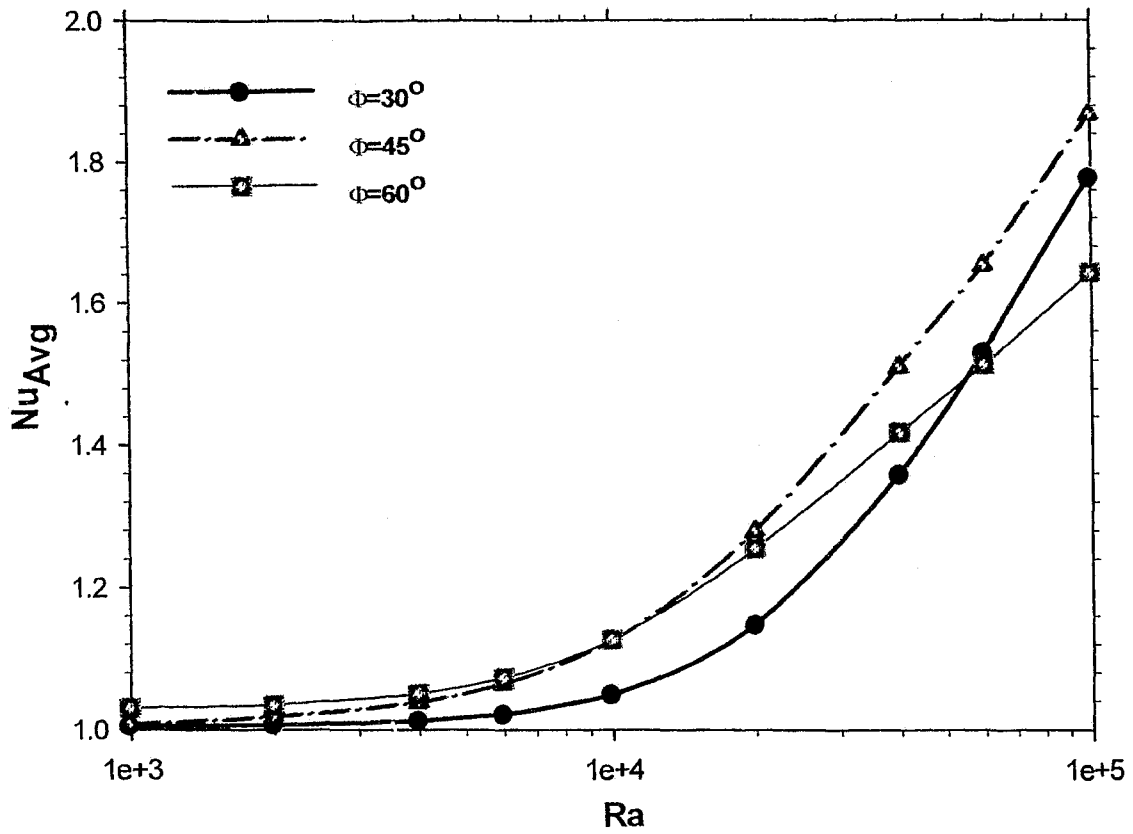
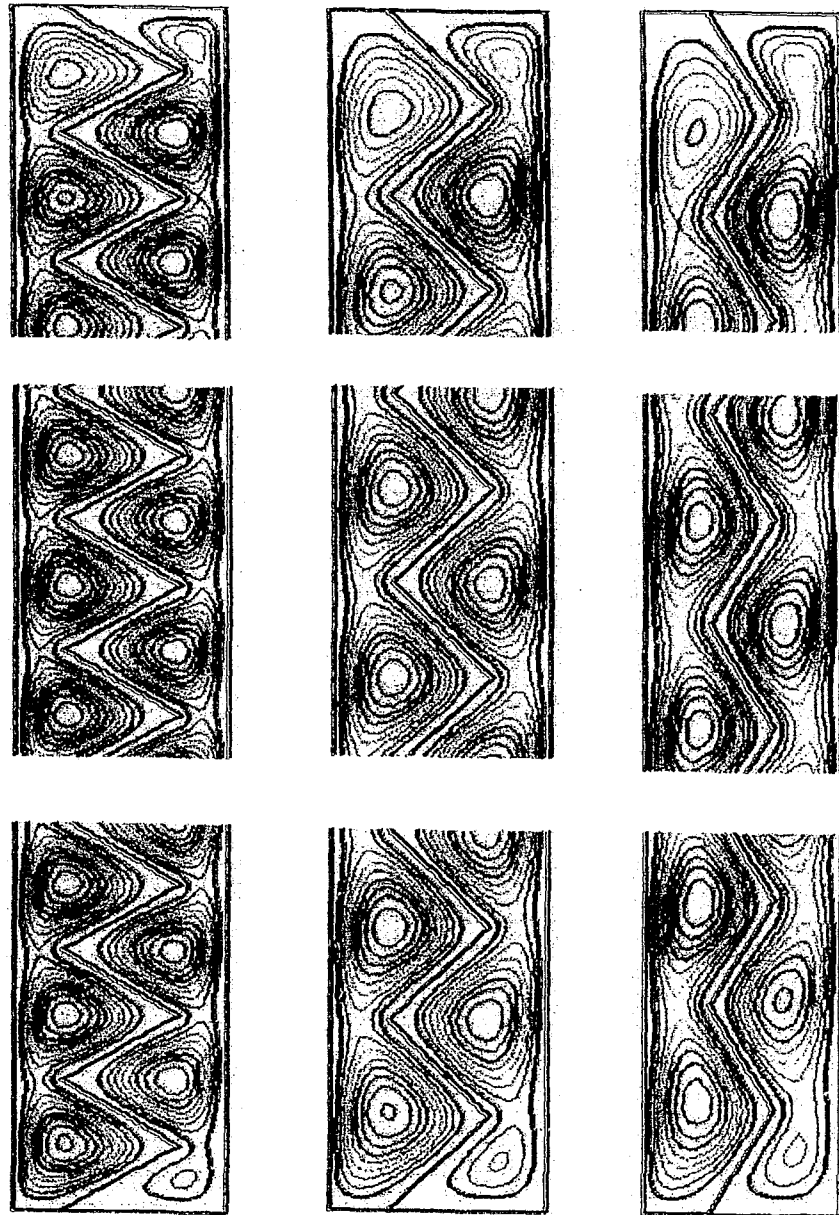


Figure 3.6 Effect of Rayleigh number on the average Nusselt Number for different blind Angle ($S=16\text{mm}$, $A=20$, $Pr=0.71$, $k_B/k_F=2.53$).



(a)

(b)

(c)

Figure 3.7 Stream function contour for different angle (a) $\Phi=30^\circ$ (max. stream function $\Psi=1.33 \times 10^{-4} \text{ m}^2/\text{s}$) (b) $\Phi=45^\circ$ (max stream function $\Psi=1.96 \times 10^{-4} \text{ m}^2/\text{s}$) (c) $\Phi=60^\circ$ (max. stream function $\Psi=2.78 \times 10^{-4} \text{ m}^2/\text{s}$) ($Ra=1 \times 10^5$, $Pr=0.7$, $A=20$, $k_B/k_F=2.53$, $S=16\text{mm}$).

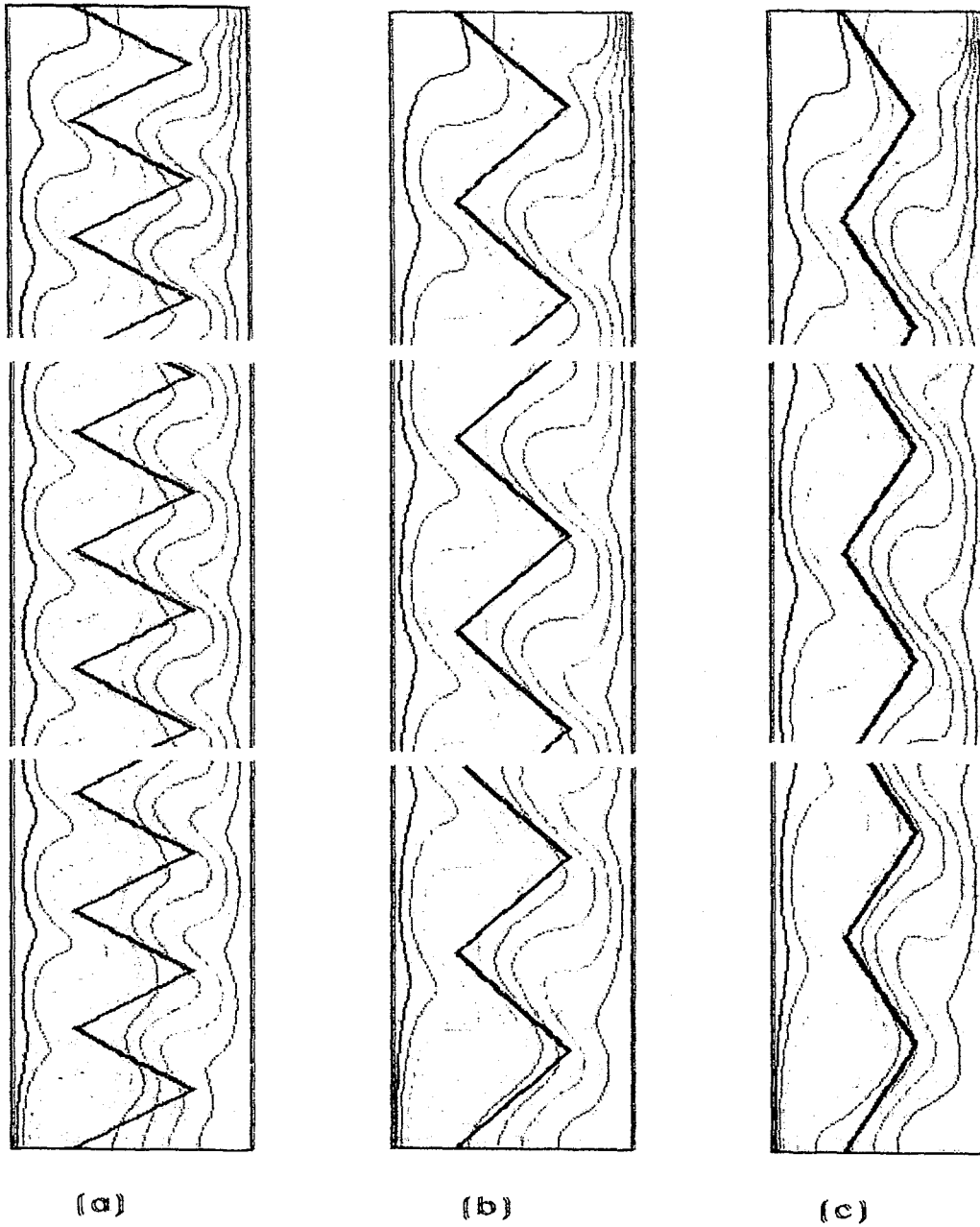


Figure 3.8 Isotherms for blind angle (a) $\Phi=30^\circ$ (b) $\Phi=45^\circ$ (c) $\Phi=60^\circ$
 ($Ra=1 \times 10^5$, $A=20$, $Pr=0.71$, $k_B/k_F=2.53$, $S=16\text{mm}$).

the blind angle has only a weak effect on the convective heat transfer rate. At higher Rayleigh numbers the behavior is complex and involves competing effects. On the one hand, increasing the blind angle increases the strength of the convective flow in the enclosure. This can be seen from the value of the maximum stream function (Figure 3.7). This effect will act to increase the convection. However, on the other hand, as the blind angle increases, the gap between the blind tips (folds) increases. As discussed previously, a wider gap prevents the flow from “penetrating” as deeply across the enclosure and increases the convective resistance. It can be seen in Figure 3.7 that there is an interplay of these two competing effects. From a practical perspective, most window applications correspond to a Rayleigh number substantially lower than $Ra=10^5$. So, for many applications, Figure 3.6 shows that the lowest blind angle ($\Phi=30^\circ$) will give the largest convective resistance. In practice, lower angles will require more blind material and a compromise will have to be made.

The effect of blind angle on the convective heat transfer has also been calculated for a higher aspect ratio enclosure, $A=40$. It was found that the results generally follow the same pattern. Given the complexity of the heat transfer behavior, it would be an interesting area for researchers to do an experimental study.

3.2.5 Effects of Aspect Ratio on Convective Heat Transfer

Aspect ratio (H/W) is an important factor in the window geometry that may affect heat transfer rate. In present study, two aspect ratios have been considered: $A=20$ and $A=40$. As mentioned earlier, these aspect ratios are only nominal values. It was necessary to adjust the height of the enclosure slightly to obtain an integer number of

blinds. Figure 3.9 shows the effect of aspect ratio on the average Nusselt number over a range of Rayleigh number for $A=20$ and $A=40$. It is interesting to note that the aspect ratio has almost no effect on the average heat transfer rate. The maximum percentage difference was 0.26%. The reason for this is because the pleated blind divides the cavity. It can be seen in the contour plots (e.g., Figure 3.4, Figure 3.7) that the velocity and temperature fields become highly periodic. As a result, increasing the height of the enclosure simply repeats the same flow pattern.

3.3 Numerical Radiation Model of the Between-Panes Pleated Blind

In this section, a conjugate convection, conduction, and radiation model is developed. This “Simplified Model” corresponds to the convective heat transfer data from the convection-only CFD model, combined with a simple one dimensional radiation model. The results of this simplified model have been compared to a full CFD simulation, which included radiation effects. The full CFD solution has been tested for grid independence. The comparison with the full CFD numerical solution has been made for summer weather conditions.

3.3.1 Simple One Dimensional Model of the Pleated Blind

As per Figure 3.10, applying a steady-state energy balance at a control volume near the blind, gives the following equation:

$$Q_{\text{CONV,HB}} + Q_{\text{RAD,HB}} = Q_{\text{CONV,BC}} + Q_{\text{RAD,BC}} \quad (3.1)$$

where $Q_{\text{CONV,HB}}$ is the convective heat transfer rate from the hot glazing to the blind and $Q_{\text{CONV,CB}}$ is the convective heat transfer rate from the blind to the cold glazing. Similarly,

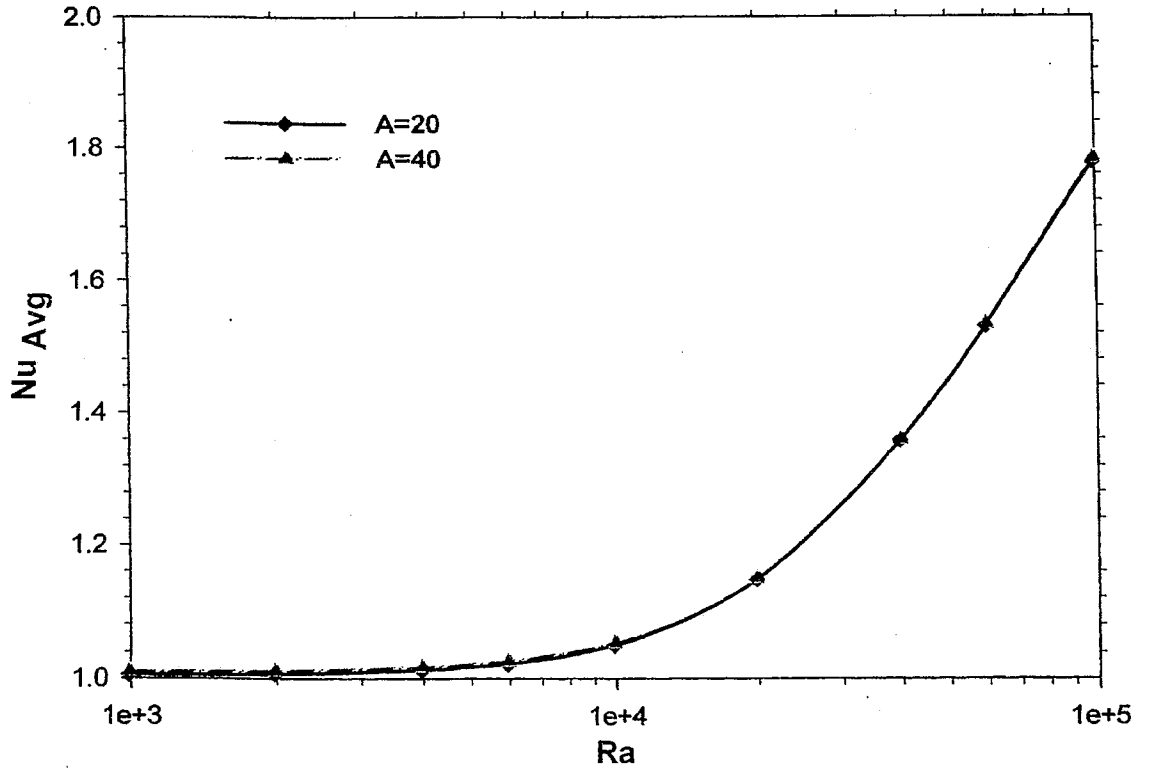


Figure 3.9 Effect of Rayleigh number on the average Nusselt for different aspect ratio ($Pr=0.71$, $\Phi=30^\circ$, $S=16\text{mm}$, $k_B/k_F=2.53$).

$Q_{RAD,HB}$ is the radiative heat transfer rate from the hot glazing to the blind and $Q_{RAD,BC}$ is the radiative heat transfer rates from the blind to the cold glazing.

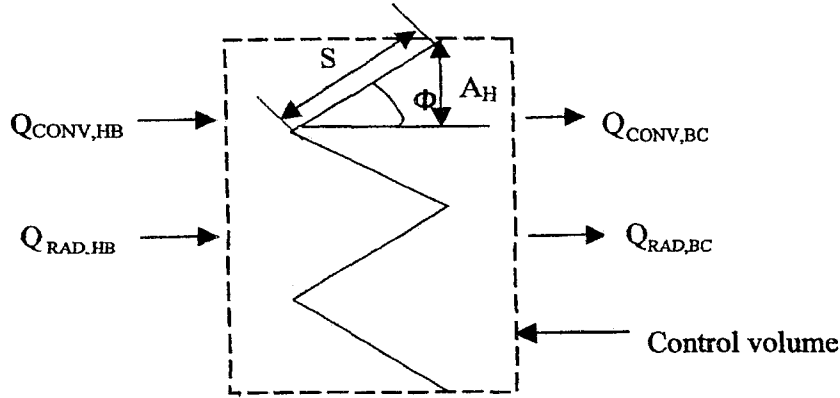


Figure 3.10 Energy balance at a control volume around the pleated blind.

The blind temperature is unknown (T_B), and must be adjusted to balance eq. (3.1). Once balanced, the U-Value is:

$$U = \frac{Q_{CONV,HB} + Q_{RAD,HB}}{A(T_H - T_C)} = \frac{Q_{CONV,BC} + Q_{RAD,BC}}{A(T_H - T_C)} \quad (3.2)$$

where T_H is hot side glazing temperature and T_C is cold side glazing temperature.

Considering a unit depth of window, the area of window is $A = H$ in the above equation.

Models of Heat Transfer Components

The convective heat transfer rate from hot glazing to the blind is calculated as:

$$Q_{CONV,HB} = h_{HB} (T_H - T_B)H \quad (3.3)$$

The convective heat transfer rate from blind to the cold glazing is calculated as:

$$Q_{CONV,BC} = h_{CB} (T_B - T_C)H \quad (3.4)$$

where h_{HB} is convective heat transfer coefficient between the hot surface and the blind and h_{CB} is the convective heat transfer coefficient between the cold surface and the blind.

In the simplified model, the heat transfer coefficients h_{HB} and h_{CB} are estimated from the

convection-only CFD model (without radiation). This is done by first calculating the total convective conductance, as follows

$$Q_{\text{CONV,TOTAL}} = h_{\text{TOTAL}} H(T_H - T_C) \quad (3.5)$$

$$h_{\text{TOTAL}} = \frac{Q_{\text{CONV,TOTAL}}}{H(T_H - T_C)} \quad (3.6)$$

where h_{TOTAL} is obtained from the convection-only CFD solution. If the blind is located centrally within the enclosure, it is reasonable to assume that the convective resistance will split equally on each side of the blind. So,

$$\frac{1}{h_{\text{CB}}} + \frac{1}{h_{\text{HB}}} = \frac{1}{h_{\text{TOTAL}}}, \quad h_{\text{CB}} = h_{\text{HB}} \quad (3.7)$$

$$h_{\text{CB}} = h_{\text{HB}} = 2h_{\text{TOTAL}}$$

Radiation Calculation

The one dimensional radiation model is based on the assumption that all surfaces may be treated as opaque, grey and diffuse. Also, it is assumed that the blind can be approximated as having a single temperature (T_B). Figure 3.11 shows the resistance network for the one-dimensional radiation heat transfer between the hot glazing and the pleated blind. In this figure, ϵ_H is emissivity of hot-side glazing surface, ϵ_B is emissivity of blind. F_{HB} is the view factor from hot surface glazing to blind.

Referring to Figure 3.10, the area of the blind is related to the area of the window as:

$$A_B \sin\Phi = A_H \quad (3.8)$$

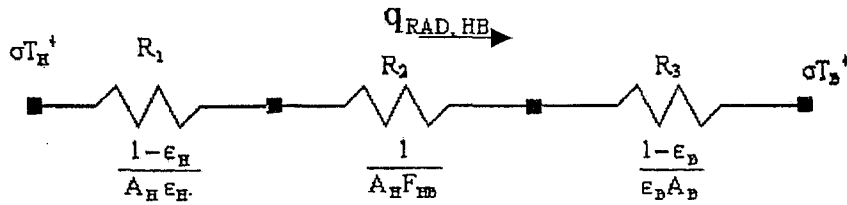


Figure 3.11 Resistance network for radiation heat transfer from hot wall to the blind.

where A_B is area of blind and A_H is the height of blind and Φ is blind angle. By reciprocity, the view factor resistance is given by:

$$\frac{1}{A_H F_{HB}} = \frac{1}{A_B F_{BH}} \quad (3.9)$$

and rearranging eq. (3.8) gives :

$$\frac{A_H}{A_B} = \sin \Phi \quad (3.10)$$

Note that the view factor from the hot glazing to the blind is approximately one:

$$F_{HB} \cong 1$$

Using the resistance network in Fig. 3.11, the radiation heat transfer rate from the hot glazing to the blind is:

$$Q_{\text{RAD, HB}} = \frac{\sigma(T_H^4 - T_B^4)}{\frac{1 - \epsilon_H}{\epsilon_H A_H} + \frac{1}{A_H F_{HB}} + \frac{1 - \epsilon_B}{\epsilon_B A_B}} \quad (3.11)$$

For unit depth, the area of the hot glazing is equal to the height of the cavity, so $A_H = H(1)$. So, substituting eq. (3.10) into eq. (3.11), gives:

$$Q_{\text{RAD,HB}} = \frac{\sigma H(T_H^4 - T_B^4)}{\frac{1}{\epsilon_H} + \frac{1 - \epsilon_B}{\epsilon_B} \sin\Phi} \quad (3.12)$$

Similarly, the radiation heat transfer rate from the blind to cold glazing can also be written as:

$$Q_{\text{RAD,BC}} = \frac{\sigma H(T_B^4 - T_C^4)}{\frac{1}{\epsilon_C} + \frac{1 - \epsilon_B}{\epsilon_B} \sin\Phi} \quad (3.13)$$

The total energy balance is convection/conduction and radiation from the hot glazing surface to the blind and the blind surface to cold glazing surface from eq. (3.1) can be written as:

$$h_{\text{HB}}H(T_H - T_B) + \frac{\sigma H(T_H^4 - T_B^4)}{\frac{1}{\epsilon_H} + \frac{1 - \epsilon_{B,1}}{\epsilon_{B,1}} \sin\Phi} = h_{\text{BC}}H(T_B - T_C) + \frac{\sigma H(T_B^4 - T_C^4)}{\frac{1}{\epsilon_C} + \frac{1 - \epsilon_{B,2}}{\epsilon_{B,2}} \sin\Phi} \quad (3.14)$$

Note in eq. (3.14) that the emissivity of the blind could be different on the hot side ($\epsilon_{B,1}$) from on the cold side ($\epsilon_{B,2}$). In many practical cases, the emissivity of both sides of the blind will be the same (i.e., $\epsilon_{B,1} = \epsilon_{B,2}$).

For each calculation, the blind temperature T_B was adjusted iteratively until the energy balance was satisfied at the blind surface, as per eq. (3.14). Once balanced, the U-Value was obtained using eq. (3.2).

In this study, the ‘‘Simplified Model’’ corresponds to: (i) the convective heat transfer data from the convection-only CFD model, combined with (ii) the one-dimensional gray-diffuse radiation model of the window and the blind.

3.3.2 Grid Independency Study for Convection/Conduction/Radiation CFD Model

The issue of independency of the grid has been studied for the conjugate convection/conduction/radiation model (full CFD model) and results are shown in Table 3.2. As can be seen from Case 1 and Case 2 in Table 3.2, increasing the number of nodes and sub-surfaces by 2.4 times changed the total heat transfer rate less than 1% and radiation heat transfer rate by 1.3%. In comparison, the convective heat transfer rate is essentially unchanged. Comparing Case 1 and Case 3, the number of nodes and sub-surfaces is increased by almost three times. The total heat transfer rate changed by 5.3% and radiation heat transfer changed by 8%, but the convective heat transfer changed by only 0.02%. Based on this testing, the full CFD model was run with a grid density comparable to case 3 (approx. 100,000 nodes).

Table 3.2 Total and radiation heat transfer data for three different grid densities ($Ra=10^4$, $Pr=0.71$, $A=20$, $\epsilon_H=0.84$, $\epsilon_B=0.8$, $\epsilon_C=0.84$, $k_B/k_F=2.53$, $S=16\text{mm}$, $T_H=305\text{K}$, $T_C=297\text{K}$).

	No. of Nodes	No. of Radiation sub surfaces	Total Heat transfer rate, Q_{hot} (W)	Total Heat Transfer, Q_{cold} (W)	Radiation Heat Transfer, Q_{hot} (W)	Radiation Heat Transfer, Q_{cold}	Convection Heat Transfer, Q_{hot} (W)	Convection Heat Transfer, Q_{cold} (W)
Case 1	35427	67808	15.07	-15.07	9.844	-9.708	5.226	-5.362
Case 2	85119	165174	15.204	-15.19	9.981	-9.835	5.223	-5.355
Case 3	106893	207712	15.92	-15.9	10.695	-10.555	5.225	-5.345

3.3.3 Comparison of the Simplified One Dimensional Model with the Full CFD Model.

It is very interesting to compare the full CFD model with the simplified model. Two cases have been considered. Case 1 is an untreated window (High-e) and Case 2 is a window with a low emissivity coating on the hot glazing (Low-e). As discussed above, in

the simplified model, the convective heat transfer coefficients were obtained from the convection-only CFD solution and the blind temperature T_B was adjusted iteratively to achieve an energy balance at the blind surface (eq. 3.12). The total heat transfer has been calculated and compared to the total heat transfer rate from the full CFD solution.

The ASHRAE summer conditions and window glazing properties were as follows:

Case 1 High-e Window

- ❖ $T_H=305K$
- ❖ $T_C=297K$
- ❖ $\epsilon_H = 0.84$
- ❖ $\epsilon_B = 0.8$
- ❖ $\epsilon_C = 0.84$

Case 2 Low-e Window

- $T_H=305K$
- $T_C=297K$
- $\epsilon_H = 0.1$
- $\epsilon_B = 0.8$
- $\epsilon_C = 0.84$

Results for case 1 (untreated, high-e window) are shown in Table 3.3. It can be seen that the simplified model works very well. The simplified model predicts the radiative and total heat transfer rates to better than 1%.

Table 3.3 Comparison results from the simplified model and the full CFD solution for an untreated window, High-e (Case 1).

	$Q_{TOTAL, H}$ (W)	$Q_{TOTAL, C}$ (W)	$Q_{RAD, H}$ (W)	$Q_{RAD, C}$ (W)
Simplified Model	14.96	-14.96	9.80	-9.68
Full CFD Model (including radiation)	15.06	-15.07	9.84	-9.71
% difference	0.686		0.33	

The results for the treated, low-e window (case 2) are shown in Table 3.4. It can be seen in Table 3.4 that the heat transfer rates predicted by the simplified model are approximately 4% lower than predicted by the full CFD simulation. This level of accuracy is acceptable for most window design applications.

Figure 3.12 shows the temperature contours and stream function for the low-e case. It can be seen from this figure that decreasing emissivity on the hot side increases the thermal resistance from hot side to blind. Note that the temperature difference between the hot glazing and the blind is much larger than the temperature difference between the blind and the cold glazing. As expected, Table 3.4 indicates that the radiation heat transfer rate is lower than the convective heat transfer rate at the hot glazing. The reverse is true at the cold (untreated) glazing.

Table 3.4 Comparison results from the simplified model and the full CFD solution for treated window, Low-e (Case 2).

	$Q_{TOTAL,H}$ (W)	$Q_{Total,C}$ (W)	$Q_{RAD,H}$ (W)	$Q_{RAD,C}$ (W)	$Q_{CONV,H}$ (W)	$Q_{CONV,C}$ (W)	U-Value
Simplified Model	9.08	-9.08	1.87	-5.86	7.21	-3.22	2.27
Full CFD Model	9.46	-9.37	1.824	-6.12	7.636	-3.25	2.36
% difference	3.5%		2.6%		4.2%		3.8%

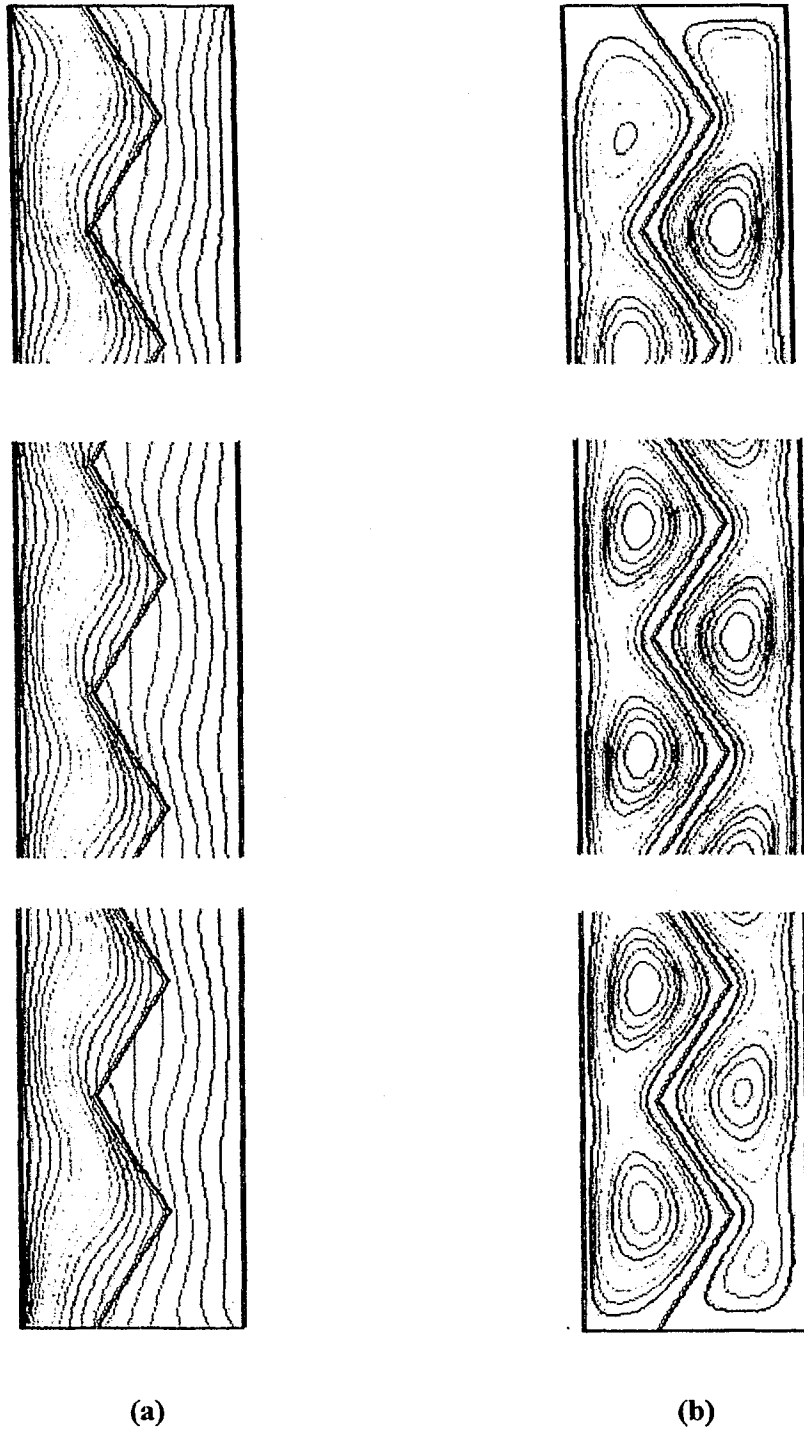


Figure 3.12 (a) Isotherms for low-e case (b) Stream function for low-e case
 ($Ra=10^4$, $Pr=0.71$, $A=20$, $S=16\text{mm}$, $\epsilon_H=0.1$, $\epsilon_B=0.8$, $\epsilon_C=0.84$, $k_B/k_F=2.53$)

CHAPTER 4: CONCLUSIONS AND RECOMMENDATIONS

4.1 Conclusions

A numerical study has been conducted that examines the effect of a pleated blind located between the panes of a double glazed window. The focus of this study was on the effect of the blind on the free convection within the window enclosure. The main results are summarized as follows:

(i) The convective heat transfer rate is not a strong function of the aspect ratio of the window enclosure ($A=H/W$). The results for $A=20$ and $A=40$ show that the aspect ratio has almost no effect on the average Nusselt number. For the geometries studied, the maximum percentage difference was found to be 0.26% over a Rayleigh number range $10^3 \leq Ra \leq 10^5$.

(ii) The type of fill gas (air, argon or krypton) has only a weak effect on the convective heat transfer rate. The maximum percentage difference for three types of fill gas was found to be 1.6%. This small difference in average Nusselt number was caused by the slight difference in conductivity ratio, since the Prandtl numbers for the three gases are essentially the same ($Pr \approx 0.7$).

(iii) As blind width (S) increases, the convective heat transfer rate was found to increase over the full range of Rayleigh number. There appear to be two reasons. As S increases, the gap between the tips of blind and the window glazing decreases, allowing the fluid on

the hot side of the enclosure to “penetrate” closer to the cold glazing. Similarly, because of blind symmetry, this geometric change also allows the fluid on the cold side of the enclosure to flow in closer proximity to the hot glazing. This geometric effect also causes stronger flow on both sides of the blind, which acts to increase the convective heat transfer.

(iv) The effect of blind angle was found to be complex. For constant blind width (S), when the blind angle (Φ) increases, the gap between the blind tips (folds) and the glazing surface increases. As discussed above, this geometric effect will tend to reduce convective heat transfer rate. However, it can be seen from the stream function values that the strength of the flow in the enclosure increases as blind angle increases. So, this behavior involves competing effects. At low Rayleigh number, near the pure conduction regime, the lowest blind angle studied ($\Phi=30^\circ$) was found to give the highest convective resistance. But, at higher Rayleigh number, this situation changed because of the competing effects discussed above.

(v) Most of the results presented in this thesis do not include the conjugate effects of thermal radiation. However, it has been shown that the data from the convection-only model can be combined with a simplified one-dimensional model to estimate the overall U-value of the enclosure. The accuracy of this simplified method was found to be sufficient for most window design applications. So, for many practical purposes, it is not necessary to include the effects of radiation in the CFD calculation. This has the benefits of reducing the computational requirements and the number of variables in the solution.

Using the procedure given in this thesis, the average Nusselt number data can be applied to a window and blind with arbitrary radiation parameters.

4.2 Recommendations

It is recognized that the current work has only a limited scope. Further research needs to be done to more fully understand the interactions between the window and blind. Recommendations for future studies are as follows:

- i) The results of the current study need to be verified experimentally. This could be done using laser interferometry and flow visualization, similar to the previous studies of Machin (1997) and Lai (2004), which were done for a Venetian blind.

- ii) In present study of inter-pane pleated blind, the pitch of the blind folds was assumed to be constant. However, in an actual window, the weight of the blind produces a significant variation in the blind pitch. Near the top of the window, the blind folds are more closely spaced than near the bottom. This variation in geometry will affect the convection to some extent. This effect needs to be studied, both numerically and experimentally.

- iii) In present study, the blind is considered to be located in center of the window enclosure. In commercial window products, the blind is sometimes located off-center in order to fit muntin bars inside the enclosure. So, the effect of off-center blind placement should be considered for future numerical and experimental study.

APPENDIX A: - FLUENT 6.0 SAMPLE INPUT FILE.

/journal file Rasesh 25.4 mm 30 deg centred (64 blinds, no glass) solver select "FLUENT 5/6"

```
/
vertex create coordinates 0 0 0
vertex create coordinates 0 0.016 0
vertex create coordinates 0 0.032 0
vertex create coordinates 0 0.048 0
vertex create coordinates 0 0.064 0
vertex create coordinates 0 0.08 0
vertex create coordinates 0 0.096 0
vertex create coordinates 0 0.112 0
vertex create coordinates 0 0.128 0
vertex create coordinates 0 0.144 0
vertex create coordinates 0 0.16 0
vertex create coordinates 0 0.176 0
vertex create coordinates 0 0.192 0
vertex create coordinates 0 0.208 0
vertex create coordinates 0 0.224 0
vertex create coordinates 0 0.24 0
vertex create coordinates 0 0.256 0
vertex create coordinates 0 0.272 0
vertex create coordinates 0 0.288 0
vertex create coordinates 0 0.304 0
vertex create coordinates 0 0.32 0
vertex create coordinates 0 0.336 0
vertex create coordinates 0 0.352 0
vertex create coordinates 0 0.368 0
vertex create coordinates 0 0.384 0
vertex create coordinates 0 0.4 0
vertex create coordinates 0 0.416 0
vertex create coordinates 0 0.432 0
vertex create coordinates 0 0.448 0
vertex create coordinates 0 0.464 0
vertex create coordinates 0 0.48 0
vertex create coordinates 0 0.496 0
vertex create coordinates 0 0.512 0
vertex create coordinates 0.005466786 0 0
vertex create coordinates 0.005466786 0.016 0
vertex create coordinates 0.005466786 0.032 0
vertex create coordinates 0.005466786 0.048 0
vertex create coordinates 0.005466786 0.064 0
vertex create coordinates 0.005466786 0.08 0
vertex create coordinates 0.005466786 0.096 0
vertex create coordinates 0.005466786 0.112 0
vertex create coordinates 0.005466786 0.128 0
vertex create coordinates 0.005466786 0.144 0
vertex create coordinates 0.005466786 0.16 0
vertex create coordinates 0.005466786 0.176 0
vertex create coordinates 0.005466786 0.192 0
vertex create coordinates 0.005466786 0.208 0
vertex create coordinates 0.005466786 0.224 0
vertex create coordinates 0.005466786 0.24 0
vertex create coordinates 0.005466786 0.256 0
vertex create coordinates 0.005466786 0.272 0
vertex create coordinates 0.005466786 0.288 0
vertex create coordinates 0.005466786 0.304 0
vertex create coordinates 0.005466786 0.32 0
vertex create coordinates 0.005466786 0.336 0
vertex create coordinates 0.005466786 0.352 0
vertex create coordinates 0.005466786 0.368 0
vertex create coordinates 0.005466786 0.384 0
vertex create coordinates 0.005466786 0.4 0
vertex create coordinates 0.005466786 0.416 0
vertex create coordinates 0.005466786 0.432 0
vertex create coordinates 0.005466786 0.448 0
vertex create coordinates 0.005466786 0.464 0
vertex create coordinates 0.005466786 0.48 0
vertex create coordinates 0.005466786 0.496 0
```

```

/
/Glass -Air Interface Left
edge create "I1L" straight "vertex.1" "vertex.2"
edge create "I2L" straight "vertex.2" "vertex.3"
edge create "I3L" straight "vertex.3" "vertex.4"
edge create "I4L" straight "vertex.4" "vertex.5"
edge create "I5L" straight "vertex.5" "vertex.6"
edge create "I6L" straight "vertex.6" "vertex.7"
edge create "I7L" straight "vertex.7" "vertex.8"
edge create "I8L" straight "vertex.8" "vertex.9"
edge create "I9L" straight "vertex.9" "vertex.10"
edge create "I10L" straight "vertex.10" "vertex.11"
edge create "I11L" straight "vertex.11" "vertex.12"
edge create "I12L" straight "vertex.12" "vertex.13"
edge create "I13L" straight "vertex.13" "vertex.14"
edge create "I14L" straight "vertex.14" "vertex.15"
edge create "I15L" straight "vertex.15" "vertex.16"
edge create "I16L" straight "vertex.16" "vertex.17"
edge create "I17L" straight "vertex.17" "vertex.18"
edge create "I18L" straight "vertex.18" "vertex.19"
edge create "I19L" straight "vertex.19" "vertex.20"
edge create "I20L" straight "vertex.20" "vertex.21"
edge create "I21L" straight "vertex.21" "vertex.22"
edge create "I22L" straight "vertex.22" "vertex.23"
edge create "I23L" straight "vertex.23" "vertex.24"
edge create "I24L" straight "vertex.24" "vertex.25"
edge create "I25L" straight "vertex.25" "vertex.26"
edge create "I26L" straight "vertex.26" "vertex.27"
edge create "I27L" straight "vertex.27" "vertex.28"
edge create "I28L" straight "vertex.28" "vertex.29"
edge create "I29L" straight "vertex.29" "vertex.30"
edge create "I30L" straight "vertex.30" "vertex.31"
edge create "I31L" straight "vertex.31" "vertex.32"
edge create "I32L" straight "vertex.32" "vertex.33"

```

```

/
/Fluid Left edges
edge create "F1L" straight "vertex.1" "vertex.34"
edge create "F2L" straight "vertex.2" "vertex.35"
edge create "F3L" straight "vertex.3" "vertex.36"
edge create "F4L" straight "vertex.4" "vertex.37"
edge create "F5L" straight "vertex.5" "vertex.38"
edge create "F6L" straight "vertex.6" "vertex.39"
edge create "F7L" straight "vertex.7" "vertex.40"
edge create "F8L" straight "vertex.8" "vertex.41"
edge create "F9L" straight "vertex.9" "vertex.42"
edge create "F10L" straight "vertex.10" "vertex.43"
edge create "F11L" straight "vertex.11" "vertex.44"
edge create "F12L" straight "vertex.12" "vertex.45"
edge create "F13L" straight "vertex.13" "vertex.46"
edge create "F14L" straight "vertex.14" "vertex.47"
edge create "F15L" straight "vertex.15" "vertex.48"
edge create "F16L" straight "vertex.16" "vertex.49"
edge create "F17L" straight "vertex.17" "vertex.50"
edge create "F18L" straight "vertex.18" "vertex.51"
edge create "F19L" straight "vertex.19" "vertex.52"
edge create "F20L" straight "vertex.20" "vertex.53"
edge create "F21L" straight "vertex.21" "vertex.54"
edge create "F22L" straight "vertex.22" "vertex.55"
edge create "F23L" straight "vertex.23" "vertex.56"
edge create "F24L" straight "vertex.24" "vertex.57"
edge create "F25L" straight "vertex.25" "vertex.58"
edge create "F26L" straight "vertex.26" "vertex.59"
edge create "F27L" straight "vertex.27" "vertex.60"
edge create "F28L" straight "vertex.28" "vertex.61"
edge create "F29L" straight "vertex.29" "vertex.62"
edge create "F30L" straight "vertex.30" "vertex.63"
edge create "F31L" straight "vertex.31" "vertex.64"
edge create "F32L" straight "vertex.32" "vertex.65"
edge create "F33L" straight "vertex.33" "vertex.66"

```

/

/Blind Left Edges

```
edge create "B1L" straight "vertex.34" "vertex.100"  
edge create "B2L" straight "vertex.100" "vertex.35"  
edge create "B3L" straight "vertex.35" "vertex.101"  
edge create "B4L" straight "vertex.101" "vertex.36"  
edge create "B5L" straight "vertex.36" "vertex.102"  
edge create "B6L" straight "vertex.102" "vertex.37"  
edge create "B7L" straight "vertex.37" "vertex.103"  
edge create "B8L" straight "vertex.103" "vertex.38"  
edge create "B9L" straight "vertex.38" "vertex.104"  
edge create "B10L" straight "vertex.104" "vertex.39"  
edge create "B11L" straight "vertex.39" "vertex.105"  
edge create "B12L" straight "vertex.105" "vertex.40"  
edge create "B13L" straight "vertex.40" "vertex.106"  
edge create "B14L" straight "vertex.106" "vertex.41"  
edge create "B15L" straight "vertex.41" "vertex.107"  
edge create "B16L" straight "vertex.107" "vertex.42"  
edge create "B17L" straight "vertex.42" "vertex.108"  
edge create "B18L" straight "vertex.108" "vertex.43"  
edge create "B19L" straight "vertex.43" "vertex.109"  
edge create "B20L" straight "vertex.109" "vertex.44"  
edge create "B21L" straight "vertex.44" "vertex.110"  
edge create "B22L" straight "vertex.110" "vertex.45"  
edge create "B23L" straight "vertex.45" "vertex.111"  
edge create "B24L" straight "vertex.111" "vertex.46"  
edge create "B25L" straight "vertex.46" "vertex.112"  
edge create "B26L" straight "vertex.112" "vertex.47"  
edge create "B27L" straight "vertex.47" "vertex.113"  
edge create "B28L" straight "vertex.113" "vertex.48"  
edge create "B29L" straight "vertex.48" "vertex.114"  
edge create "B30L" straight "vertex.114" "vertex.49"  
edge create "B31L" straight "vertex.49" "vertex.115"  
edge create "B32L" straight "vertex.115" "vertex.50"  
edge create "B33L" straight "vertex.50" "vertex.116"  
edge create "B34L" straight "vertex.116" "vertex.51"  
edge create "B35L" straight "vertex.51" "vertex.117"  
edge create "B36L" straight "vertex.117" "vertex.52"  
edge create "B37L" straight "vertex.52" "vertex.118"  
edge create "B38L" straight "vertex.118" "vertex.53"  
edge create "B39L" straight "vertex.53" "vertex.119"  
edge create "B40L" straight "vertex.119" "vertex.54"  
edge create "B41L" straight "vertex.54" "vertex.120"  
edge create "B42L" straight "vertex.120" "vertex.55"  
edge create "B43L" straight "vertex.55" "vertex.121"  
edge create "B44L" straight "vertex.121" "vertex.56"  
edge create "B45L" straight "vertex.56" "vertex.122"  
edge create "B46L" straight "vertex.122" "vertex.57"  
edge create "B47L" straight "vertex.57" "vertex.123"  
edge create "B48L" straight "vertex.123" "vertex.58"  
edge create "B49L" straight "vertex.58" "vertex.124"  
edge create "B50L" straight "vertex.124" "vertex.59"  
edge create "B51L" straight "vertex.59" "vertex.125"  
edge create "B52L" straight "vertex.125" "vertex.60"  
edge create "B53L" straight "vertex.60" "vertex.126"  
edge create "B54L" straight "vertex.126" "vertex.61"  
edge create "B55L" straight "vertex.61" "vertex.127"  
edge create "B56L" straight "vertex.127" "vertex.62"  
edge create "B57L" straight "vertex.62" "vertex.128"  
edge create "B58L" straight "vertex.128" "vertex.63"  
edge create "B59L" straight "vertex.63" "vertex.129"  
edge create "B60L" straight "vertex.129" "vertex.64"  
edge create "B61L" straight "vertex.64" "vertex.130"  
edge create "B62L" straight "vertex.130" "vertex.65"  
edge create "B63L" straight "vertex.65" "vertex.131"  
edge create "B64L" straight "vertex.131" "vertex.66"
```

/Blind bottom edges

```
edge create "B1B" straight "vertex.34" "vertex.67"
```

```

edge create "B2B" straight "vertex.35" "vertex.68"
edge create "B3B" straight "vertex.36" "vertex.69"
edge create "B4B" straight "vertex.37" "vertex.70"
edge create "B5B" straight "vertex.38" "vertex.71"
edge create "B6B" straight "vertex.39" "vertex.72"
edge create "B7B" straight "vertex.40" "vertex.73"
edge create "B8B" straight "vertex.41" "vertex.74"
edge create "B9B" straight "vertex.42" "vertex.75"
edge create "B10B" straight "vertex.43" "vertex.76"
edge create "B11B" straight "vertex.44" "vertex.77"
edge create "B12B" straight "vertex.45" "vertex.78"
edge create "B13B" straight "vertex.46" "vertex.79"
edge create "B14B" straight "vertex.47" "vertex.80"
edge create "B15B" straight "vertex.48" "vertex.81"
edge create "B16B" straight "vertex.49" "vertex.82"
edge create "B17B" straight "vertex.50" "vertex.83"
edge create "B18B" straight "vertex.51" "vertex.84"
edge create "B19B" straight "vertex.52" "vertex.85"
edge create "B20B" straight "vertex.53" "vertex.86"
edge create "B21B" straight "vertex.54" "vertex.87"
edge create "B22B" straight "vertex.55" "vertex.88"
edge create "B23B" straight "vertex.56" "vertex.89"
edge create "B24B" straight "vertex.57" "vertex.90"
edge create "B25B" straight "vertex.58" "vertex.91"
edge create "B26B" straight "vertex.59" "vertex.92"
edge create "B27B" straight "vertex.60" "vertex.93"
edge create "B28B" straight "vertex.61" "vertex.94"
edge create "B29B" straight "vertex.62" "vertex.95"
edge create "B30B" straight "vertex.63" "vertex.96"
edge create "B31B" straight "vertex.64" "vertex.97"
edge create "B32B" straight "vertex.65" "vertex.98"
edge create "B33B" straight "vertex.66" "vertex.99"

```

/Blind Top edges

```

edge create "B1T" straight "vertex.100" "vertex.132"
edge create "B2T" straight "vertex.101" "vertex.133"
edge create "B3T" straight "vertex.102" "vertex.134"
edge create "B4T" straight "vertex.103" "vertex.135"
edge create "B5T" straight "vertex.104" "vertex.136"
edge create "B6T" straight "vertex.105" "vertex.137"
edge create "B7T" straight "vertex.106" "vertex.138"
edge create "B8T" straight "vertex.107" "vertex.139"
edge create "B9T" straight "vertex.108" "vertex.140"
edge create "B10T" straight "vertex.109" "vertex.141"
edge create "B11T" straight "vertex.110" "vertex.142"
edge create "B12T" straight "vertex.111" "vertex.143"
edge create "B13T" straight "vertex.112" "vertex.144"
edge create "B14T" straight "vertex.113" "vertex.145"
edge create "B15T" straight "vertex.114" "vertex.146"
edge create "B16T" straight "vertex.115" "vertex.147"
edge create "B17T" straight "vertex.116" "vertex.148"
edge create "B18T" straight "vertex.117" "vertex.149"
edge create "B19T" straight "vertex.118" "vertex.150"
edge create "B20T" straight "vertex.119" "vertex.151"
edge create "B21T" straight "vertex.120" "vertex.152"
edge create "B22T" straight "vertex.121" "vertex.153"
edge create "B23T" straight "vertex.122" "vertex.154"
edge create "B24T" straight "vertex.123" "vertex.155"
edge create "B25T" straight "vertex.124" "vertex.156"
edge create "B26T" straight "vertex.125" "vertex.157"
edge create "B27T" straight "vertex.126" "vertex.158"
edge create "B28T" straight "vertex.127" "vertex.159"
edge create "B29T" straight "vertex.128" "vertex.160"
edge create "B30T" straight "vertex.129" "vertex.161"
edge create "B31T" straight "vertex.130" "vertex.162"
edge create "B32T" straight "vertex.131" "vertex.163"

```

/

/Glass-Air Interface Right

```

edge create "IIR" straight "vertex.164" "vertex.165"

```

edge create "I2R" straight "vertex.165" "vertex.166"
 edge create "I3R" straight "vertex.166" "vertex.167"
 edge create "I4R" straight "vertex.167" "vertex.168"
 edge create "I5R" straight "vertex.168" "vertex.169"
 edge create "I6R" straight "vertex.169" "vertex.170"
 edge create "I7R" straight "vertex.170" "vertex.171"
 edge create "I8R" straight "vertex.171" "vertex.172"
 edge create "I9R" straight "vertex.172" "vertex.173"
 edge create "I10R" straight "vertex.173" "vertex.174"
 edge create "I11R" straight "vertex.174" "vertex.175"
 edge create "I12R" straight "vertex.175" "vertex.176"
 edge create "I13R" straight "vertex.176" "vertex.177"
 edge create "I14R" straight "vertex.177" "vertex.178"
 edge create "I15R" straight "vertex.178" "vertex.179"
 edge create "I16R" straight "vertex.179" "vertex.180"
 edge create "I17R" straight "vertex.180" "vertex.181"
 edge create "I18R" straight "vertex.181" "vertex.182"
 edge create "I19R" straight "vertex.182" "vertex.183"
 edge create "I20R" straight "vertex.183" "vertex.184"
 edge create "I21R" straight "vertex.184" "vertex.185"
 edge create "I22R" straight "vertex.185" "vertex.186"
 edge create "I23R" straight "vertex.186" "vertex.187"
 edge create "I24R" straight "vertex.187" "vertex.188"
 edge create "I25R" straight "vertex.188" "vertex.189"
 edge create "I26R" straight "vertex.189" "vertex.190"
 edge create "I27R" straight "vertex.190" "vertex.191"
 edge create "I28R" straight "vertex.191" "vertex.192"
 edge create "I29R" straight "vertex.192" "vertex.193"
 edge create "I30R" straight "vertex.193" "vertex.194"
 edge create "I31R" straight "vertex.194" "vertex.195"
 edge create "I32R" straight "vertex.195" "vertex.196"

/
 /Fluid right edges

edge create "F1R" straight "vertex.67" "vertex.164"
 edge create "F2R" straight "vertex.68" "vertex.165"
 edge create "F3R" straight "vertex.69" "vertex.166"
 edge create "F4R" straight "vertex.70" "vertex.167"
 edge create "F5R" straight "vertex.71" "vertex.168"
 edge create "F6R" straight "vertex.72" "vertex.169"
 edge create "F7R" straight "vertex.73" "vertex.170"
 edge create "F8R" straight "vertex.74" "vertex.171"
 edge create "F9R" straight "vertex.75" "vertex.172"
 edge create "F10R" straight "vertex.76" "vertex.173"
 edge create "F11R" straight "vertex.77" "vertex.174"
 edge create "F12R" straight "vertex.78" "vertex.175"
 edge create "F13R" straight "vertex.79" "vertex.176"
 edge create "F14R" straight "vertex.80" "vertex.177"
 edge create "F15R" straight "vertex.81" "vertex.178"
 edge create "F16R" straight "vertex.82" "vertex.179"
 edge create "F17R" straight "vertex.83" "vertex.180"
 edge create "F18R" straight "vertex.84" "vertex.181"
 edge create "F19R" straight "vertex.85" "vertex.182"
 edge create "F20R" straight "vertex.86" "vertex.183"
 edge create "F21R" straight "vertex.87" "vertex.184"
 edge create "F22R" straight "vertex.88" "vertex.185"
 edge create "F23R" straight "vertex.89" "vertex.186"
 edge create "F24R" straight "vertex.90" "vertex.187"
 edge create "F25R" straight "vertex.91" "vertex.188"
 edge create "F26R" straight "vertex.92" "vertex.189"
 edge create "F27R" straight "vertex.93" "vertex.190"
 edge create "F28R" straight "vertex.94" "vertex.191"
 edge create "F29R" straight "vertex.95" "vertex.192"
 edge create "F30R" straight "vertex.96" "vertex.193"
 edge create "F31R" straight "vertex.97" "vertex.194"
 edge create "F32R" straight "vertex.98" "vertex.195"
 edge create "F33R" straight "vertex.99" "vertex.196"

/
 /Blind right edges

```

edge create "B1R" straight "vertex.67" "vertex.132"
edge create "B2R" straight "vertex.132" "vertex.68"
edge create "B3R" straight "vertex.68" "vertex.133"
edge create "B4R" straight "vertex.133" "vertex.69"
edge create "B5R" straight "vertex.69" "vertex.134"
edge create "B6R" straight "vertex.134" "vertex.70"
edge create "B7R" straight "vertex.70" "vertex.135"
edge create "B8R" straight "vertex.135" "vertex.71"
edge create "B9R" straight "vertex.71" "vertex.136"
edge create "B10R" straight "vertex.136" "vertex.72"
edge create "B11R" straight "vertex.72" "vertex.137"
edge create "B12R" straight "vertex.137" "vertex.73"
edge create "B13R" straight "vertex.73" "vertex.138"
edge create "B14R" straight "vertex.138" "vertex.74"
edge create "B15R" straight "vertex.74" "vertex.139"
edge create "B16R" straight "vertex.139" "vertex.75"
edge create "B17R" straight "vertex.75" "vertex.140"
edge create "B18R" straight "vertex.140" "vertex.76"
edge create "B19R" straight "vertex.76" "vertex.141"
edge create "B20R" straight "vertex.141" "vertex.77"
edge create "B21R" straight "vertex.77" "vertex.142"
edge create "B22R" straight "vertex.142" "vertex.78"
edge create "B23R" straight "vertex.78" "vertex.143"
edge create "B24R" straight "vertex.143" "vertex.79"
edge create "B25R" straight "vertex.79" "vertex.144"
edge create "B26R" straight "vertex.144" "vertex.80"
edge create "B27R" straight "vertex.80" "vertex.145"
edge create "B28R" straight "vertex.145" "vertex.81"
edge create "B29R" straight "vertex.81" "vertex.146"
edge create "B30R" straight "vertex.146" "vertex.82"
edge create "B31R" straight "vertex.82" "vertex.147"
edge create "B32R" straight "vertex.147" "vertex.83"
edge create "B33R" straight "vertex.83" "vertex.148"
edge create "B34R" straight "vertex.148" "vertex.84"
edge create "B35R" straight "vertex.84" "vertex.149"
edge create "B36R" straight "vertex.149" "vertex.85"
edge create "B37R" straight "vertex.85" "vertex.150"
edge create "B38R" straight "vertex.150" "vertex.86"
edge create "B39R" straight "vertex.86" "vertex.151"
edge create "B40R" straight "vertex.151" "vertex.87"
edge create "B41R" straight "vertex.87" "vertex.152"
edge create "B42R" straight "vertex.152" "vertex.88"
edge create "B43R" straight "vertex.88" "vertex.153"
edge create "B44R" straight "vertex.153" "vertex.89"
edge create "B45R" straight "vertex.89" "vertex.154"
edge create "B46R" straight "vertex.154" "vertex.90"
edge create "B47R" straight "vertex.90" "vertex.155"
edge create "B48R" straight "vertex.155" "vertex.91"
edge create "B49R" straight "vertex.91" "vertex.156"
edge create "B50R" straight "vertex.156" "vertex.92"
edge create "B51R" straight "vertex.92" "vertex.157"
edge create "B52R" straight "vertex.157" "vertex.93"
edge create "B53R" straight "vertex.93" "vertex.158"
edge create "B54R" straight "vertex.158" "vertex.94"
edge create "B55R" straight "vertex.94" "vertex.159"
edge create "B56R" straight "vertex.159" "vertex.95"
edge create "B57R" straight "vertex.95" "vertex.160"
edge create "B58R" straight "vertex.160" "vertex.96"
edge create "B59R" straight "vertex.96" "vertex.161"
edge create "B60R" straight "vertex.161" "vertex.97"
edge create "B61R" straight "vertex.97" "vertex.162"
edge create "B62R" straight "vertex.162" "vertex.98"
edge create "B63R" straight "vertex.98" "vertex.163"
edge create "B64R" straight "vertex.163" "vertex.99"

```

/Fluid Faces

```

face create "F1" wireframe "I1L" "F1L" "F2L" "B1L" "B2L" real
face create "F2" wireframe "I1R" "F1R" "F2R" "B1R" "B2R" real
face create "F3" wireframe "I2L" "F2L" "F3L" "B3L" "B4L" real
face create "F4" wireframe "I2R" "F2R" "F3R" "B3R" "B4R" real

```

```

face create "F5" wireframe "I3L""F3L""F4L""B5L""B6L" real
face create "F6" wireframe "I3R""F3R""F4R""B5R""B6R" real
face create "F7" wireframe "I4L""F4L""F5L" "B7L""B8L" real
face create "F8" wireframe "I4R""F4R" "F5R""B7R" "B8R" real
face create "F9" wireframe "I5L""F5L" "F6L""B9L""B10L" real
face create "F10" wireframe "I5R""F5R""F6R""B9R""B10R" real
face create "F11" wireframe "I6L""F6L" "F7L""B11L""B12L" real
face create "F12" wireframe "I6R""F6R""F7R""B11R""B12R" real
face create "F13" wireframe "I7L""F7L""F8L""B13L""B14L" real
face create "F14" wireframe "I7R""F7R""F8R" "B13R""B14R" real
face create "F15" wireframe "I8L" "F8L" "F9L" "B15L""B16L" real
face create "F16" wireframe "I8R""F8R" "F9R""B15R""B16R" real
face create "F17" wireframe "I9L""F9L""F10L""B17L""B18L" real
face create "F18" wireframe "I9R""F9R""F10R""B17R""B18R" real
face create "F19" wireframe "I10L""F10L""F11L""B19L""B20L" real
face create "F20" wireframe "I10R""F10R""F11R""B19R""B20R" real
face create "F21" wireframe "I11L""F11L""F12L""B21L""B22L" real
face create "F22" wireframe "I11R""F11R" "F12R" "B21R""B22R" real
face create "F23" wireframe "I12L""F12L""F13L""B23L""B24L" real
face create "F24" wireframe "I12R""F12R""F13R""B23R""B24R" real
face create "F25" wireframe "I13L""F13L""F14L""B25L""B26L" real
face create "F26" wireframe "I13R""F13R""F14R""B25R""B26R" real
face create "F27" wireframe "I14L""F14L""F15L""B27L""B28L" real
face create "F28" wireframe "I14R""F14R""F15R""B27R""B28R" real
face create "F29" wireframe "I15L""F15L""F16L""B29L" "B30L" real
face create "F30" wireframe "I15R""F15R""F16R" "B29R" "B30R" real
face create "F31" wireframe "I16L""F16L""F17L""B31L""B32L" real
face create "F32" wireframe "I16R""F16R""F17R""B31R""B32R" real
face create "F33" wireframe "I17L""F17L""F18L""B33L""B34L" real
face create "F34" wireframe "I17R""F17R""F18R""B33R""B34R" real
face create "F35" wireframe "I18L""F18L""F19L""B35L""B36L" real
face create "F36" wireframe "I18R""F18R""F19R""B35R""B36R" real
face create "F37" wireframe "I19L""F19L""F20L""B37L""B38L" real
face create "F38" wireframe "I19R""F19R""F20R""B37R""B38R" real
face create "F39" wireframe "I20L""F20L""F21L""B39L""B40L" real
face create "F40" wireframe "I20R""F20R""F21R""B39R""B40R" real
face create "F41" wireframe "I21L""F21L""F22L""B41L""B42L" real
face create "F42" wireframe "I21R""F21R""F22R""B41R""B42R" real
face create "F43" wireframe "I22L""F22L""F23L""B43L""B44L" real
face create "F44" wireframe "I22R""F22R""F23R""B43R""B44R" real
face create "F45" wireframe "I23L""F23L""F24L""B45L""B46L" real
face create "F46" wireframe "I23R""F23R""F24R""B45R""B46R" real
face create "F47" wireframe "I24L""F24L""F25L""B47L""B48L" real
face create "F48" wireframe "I24R""F24R""F25R""B47R""B48R" real
face create "F49" wireframe "I25L""F25L""F26L""B49L""B50L" real
face create "F50" wireframe "I25R""F25R""F26R""B49R""B50R" real
face create "F51" wireframe "I26L""F26L""F27L""B51L""B52L" real
face create "F52" wireframe "I26R""F26R""F27R""B51R""B52R" real
face create "F53" wireframe "I27L""F27L""F28L""B53L""B54L" real
face create "F54" wireframe "I27R""F27R""F28R""B53R""B54R" real
face create "F55" wireframe "I28L""F28L""F29L""B55L""B56L" real
face create "F56" wireframe "I28R""F28R""F29R""B55R""B56R" real
face create "F57" wireframe "I29L""F29L""F30L""B57L""B58L" real
face create "F58" wireframe "I29R""F29R""F30R""B57R""B58R" real
face create "F59" wireframe "I30L""F30L""F31L""B59L""B60L" real
face create "F60" wireframe "I30R""F30R""F31R""B59R""B60R" real
face create "F61" wireframe "I31L""F31L""F32L""B61L""B62L" real
face create "F62" wireframe "I31R""F31R""F32R""B61R""B62R" real
face create "F63" wireframe "I32L""F32L""F33L""B63L""B64L" real
face create "F64" wireframe "I32R""F32R""F33R""B63R""B64R" real

```

/

/Blind face

```

face create "B1" wire frame "B1B""B1L""B1R""B1T" real
face create "B2" wireframe "B1T""B2L""B2R""B2B" real
face create "B3" wireframe "B2B""B3L""B3R""B2T" real
face create "B4" wireframe "B2T""B4L""B4R""B3B" real
face create "B5" wireframe "B3B""B5L""B5R""B3T" real
face create "B6" wireframe "B3T""B6L""B6R""B4B" real
face create "B7" wireframe "B4B""B7L""B7R""B4T" real

```

face create "B8" wireframe"B4T""B8L""B8R""B5B"real
 face create "B9" wireframe"B5B""B9L""B9R""B5T"real
 face create "B10" wireframe"B5T""B10L""B10R""B6B"real
 face create "B11" wireframe"B6B""B11L""B11R""B6T"real
 face create "B12" wireframe"B6T""B12L""B12R""B7B"real
 face create "B13" wireframe"B7B""B13L""B13R""B7T"real
 face create "B14" wireframe"B7T""B14L""B14R""B8B"real
 face create "B15" wireframe"B8B""B15L""B15R""B8T"real
 face create "B16" wireframe"B8T""B16L""B16R""B9B"real
 face create "B17" wireframe"B9B""B17L""B17R""B9T"real
 face create "B18" wireframe"B9T""B18L""B18R""B10B"real
 face create "B19" wireframe"B10B""B19L""B19R""B10T"real
 face create "B20" wireframe"B10T""B20L""B20R""B11B"real
 face create "B21" wireframe"B11B""B21L""B21R""B11T"real
 face create "B22" wireframe"B11T""B22L""B22R""B12B"real
 face create "B23" wireframe"B12B""B23L""B23R""B12T"real
 face create "B24" wireframe"B12T""B24L""B24R""B13B"real
 face create "B25" wireframe"B13B""B25L""B25R""B13T"real
 face create "B26" wireframe"B13T""B26L""B26R""B14B"real
 face create "B27" wireframe"B14B""B27L""B27R""B14T"real
 face create "B28" wireframe"B14T""B28L""B28R""B15B"real
 face create "B29" wireframe"B15B""B29L""B29R""B15T"real
 face create "B30" wireframe"B15T""B30L""B30R""B16B"real
 face create "B31" wireframe"B16B""B31L""B31R""B16T"real
 face create "B32" wireframe"B16T""B32L""B32R""B17B"real
 face create "B33" wireframe"B17B""B33L""B33R""B17T"real
 face create "B34" wireframe"B17T""B34L""B34R""B18B"real
 face create "B35" wireframe"B18B""B35L""B35R""B18T"real
 face create "B36" wireframe"B18T""B36L""B36R""B19B"real
 face create "B37" wireframe"B19B""B37L""B37R""B19T"real
 face create "B38" wireframe"B19T""B38L""B38R""B20B"real
 face create "B39" wireframe"B20B""B39L""B39R""B20T"real
 face create "B40" wireframe"B20T""B40L""B40R""B21B"real
 face create "B41" wireframe"B21B""B41L""B41R""B21T"real
 face create "B42" wireframe"B21T""B42L""B42R""B22B"real
 face create "B43" wireframe"B22B""B43L""B43R""B22T"real
 face create "B44" wireframe"B22T""B44L""B44R""B23B"real
 face create "B45" wireframe"B23B""B45L""B45R""B23T"real
 face create "B46" wireframe"B23T""B46L""B46R""B24B"real
 face create "B47" wireframe"B24B""B47L""B47R""B24T"real
 face create "B48" wireframe"B24T""B48L""B48R""B25B"real
 face create "B49" wireframe"B25B""B49L""B49R""B25T"real
 face create "B50" wireframe"B25T""B50L""B50R""B26B"real
 face create "B51" wireframe"B26B""B51L""B51R""B26T"real
 face create "B52" wireframe"B26T""B52L""B52R""B27B"real
 face create "B53" wireframe"B27B""B53L""B53R""B27T"real
 face create "B54" wireframe"B27T""B54L""B54R""B28B"real
 face create "B55" wireframe"B28B""B55L""B55R""B28T"real
 face create "B56" wireframe"B28T""B56L""B56R""B29B"real
 face create "B57" wireframe"B29B""B57L""B57R""B29T"real
 face create "B58" wireframe"B29T""B58L""B58R""B30B"real
 face create "B59" wireframe"B30B""B59L""B59R""B30T"real
 face create "B60" wireframe"B30T""B60L""B60R""B31B"real
 face create "B61" wireframe"B31B""B61L""B61R""B31T"real
 face create "B62" wireframe"B31T""B62L""B62R""B32B"real
 face create "B63" wireframe"B32B""B63L""B63R""B32T"real
 face create "B64" wireframe"B32T""B64L""B64R""B33B"real

APPENDIX B:- Selected data for Nusselt number and Rayleigh number for different blind geometry.

Table B1 Nusselt number data for different blind angle

Ra	$\Phi = 30^\circ$				$\Phi = 45^\circ$				$\Phi = 60^\circ$			
	q_{hot}	q_{cold}	q_{Avg}	Nu	q_{hot}	q_{cold}	q_{Avg}	Nu	q_{hot}	q_{cold}	q_{Avg}	Nu
1000	0.528	-0.528	0.528	1.007	0.513	-0.514	0.514	1.009	0.570	-0.571	0.570	1.031
2000	0.529	-0.528	0.529	1.008	0.519	-0.519	0.519	1.020	0.572	-0.573	0.573	1.035
4000	0.532	-0.532	0.532	1.014	0.529	-0.529	0.529	1.039	0.581	-0.581	0.581	1.051
6000	0.536	-0.536	0.536	1.023	0.542	-0.542	0.542	1.065	0.593	-0.594	0.593	1.073
10000	0.551	-0.551	0.551	1.051	0.573	-0.573	0.573	1.126	0.623	-0.624	0.623	1.127
20000	0.603	-0.603	0.603	1.150	0.652	-0.652	0.652	1.280	0.695	-0.695	0.695	1.256
40000	0.713	-0.713	0.713	1.360	0.770	-0.770	0.770	1.512	0.785	-0.785	0.785	1.419
60000	0.803	-0.803	0.803	1.532	0.842	-0.842	0.842	1.654	0.838	-0.838	0.838	1.515
100000	0.933	-0.933	0.933	1.779	0.951	-0.951	0.951	1.868	0.909	-0.909	0.909	1.643

Table B2 Nusselt number data for different blind width

Ra	S=0.014				S=0.016				S=0.018			
	q_{hot} (W)	q_{cold} (W)	q_{Avg} (W)	Nu	q_{hot} (W)	q_{cold} (W)	q_{Avg} (W)	Nu	q_{hot} (W)	q_{cold} (W)	q_{Avg} (W)	Nu
1000	0.523	-0.521	0.522	1.027	0.529	-0.527	0.528	1.014	0.606	-0.591	0.599	1.017
2000	0.524	-0.520	0.522	1.028	0.529	-0.528	0.528	1.015	0.600	-0.596	0.598	1.015
4000	0.525	-0.523	0.524	1.031	0.532	-0.531	0.532	1.022	0.604	-0.602	0.603	1.024
10000	0.536	-0.536	0.536	1.055	0.552	-0.551	0.551	1.059	0.633	-0.633	0.633	1.075
20000	0.571	-0.571	0.571	1.124	0.605	-0.605	0.605	1.162	0.708	-0.708	0.708	1.203
40000	0.656	-0.655	0.656	1.290	0.717	-0.717	0.717	1.377	0.854	-0.854	0.854	1.449
60000	0.730	-0.730	0.730	1.436	0.804	-0.805	0.804	1.546	0.967	-0.963	0.965	1.639
100000	0.838	-0.838	0.838	1.649	0.938	-0.938	0.938	1.802	1.132	-1.132	1.132	1.922

Table B3 Nusselt number data for different filled gas.

Air				Krypton				Argon			
q_{hot} (W)	q_{cold} (W)	q_{Avg} (W)	Nu	$q_{hot}(W)$	q_{cold} (W)	q_{Avg} (W)	Nu	q_{hot} (W)	q_{cold} (W)	q_{Avg} (W)	Nu
0.513	-0.514	0.514	1.013	0.193	-0.193	0.193	1.027	0.357	-0.357	0.357	1.016
0.519	-0.519	0.519	1.024	0.194	-0.194	0.194	1.031	0.359	-0.359	0.359	1.020
0.529	-0.529	0.529	1.043	0.197	-0.197	0.197	1.047	0.364	-0.364	0.364	1.036
0.542	-0.542	0.542	1.069	0.201	-0.201	0.201	1.071	0.373	-0.373	0.373	1.059
0.573	-0.573	0.573	1.131	0.213	-0.213	0.213	1.133	0.394	-0.394	0.394	1.119
0.652	-0.652	0.652	1.285	0.243	-0.243	0.243	1.294	0.450	-0.450	0.450	1.279
0.770	-0.770	0.770	1.518	0.287	-0.287	0.287	1.527	0.532	-0.532	0.532	1.513
0.842	-0.842	0.842	1.661	0.315	-0.315	0.315	1.676	0.585	-0.585	0.585	1.662
0.951	-0.951	0.951	1.875	0.349	-0.349	0.349	1.858	0.649	-0.649	0.649	1.845

Table B4 Nusselt number data for different aspect ratio

Ra	Aspect Ratio = 20				Aspect Ratio = 40			
	$q_{hot}(W)$	$q_{cold}(W)$	$q_{Avg}(W)$	Nu	$q_{hot}(W)$	$q_{cold}(W)$	$q_{Avg}(W)$	Nu
1000	0.5280	-0.5275	0.5278	1.0066	1.0615	-1.0586	1.0601	1.0110
2000	0.5286	-0.5284	0.5285	1.0080	1.0618	-1.0612	1.0615	1.0123
4000	0.5316	-0.5316	0.5316	1.0139	1.0674	-1.0673	1.0674	1.0179
6000	0.5364	-0.5364	0.5364	1.0231	1.0769	-1.0768	1.0769	1.0270
10000	0.5509	-0.5509	0.5509	1.0508	1.1051	-1.1051	1.1051	1.0539
20000	0.6027	-0.6027	0.6027	1.1496	1.2070	-1.2070	1.2070	1.1511
40000	0.7129	-0.7129	0.7129	1.3597	1.4268	-1.4268	1.4268	1.3607
60000	0.8030	-0.8031	0.8031	1.5317	1.6081	-1.6081	1.6081	1.5336
100000	0.9327	-0.9328	0.9328	1.7791	1.8705	-1.8705	1.8705	1.7838

Table B5 Nusselt number data for different blind conductivity

Ra	$k_{ratio,1} = k_{cotton}/k_{air}=2.53$				$k_{ratio,2} = k_{xyz}^*/k_{air}=42.9$			
	q_{hot}	q_{cold}	q_{Avg}	Nu	q_{hot}	q_{cold}	q_{Avg}	Nu
1000	0.483	-0.483	0.483	1.012	0.559	-0.558	0.559	1.170
2000	0.484	-0.483	0.484	1.015	0.559	-0.558	0.559	1.171
4000	0.487	-0.484	0.485	1.021	0.561	-0.560	0.561	1.175
10000	0.504	-0.503	0.504	1.056	0.576	-0.576	0.576	1.206
20000	0.551	-0.550	0.551	1.154	0.617	-0.618	0.617	1.294
40000	0.644	-0.644	0.644	1.350	0.708	-0.707	0.708	1.483
60000	0.736	-0.736	0.736	1.542	0.780	-0.780	0.780	1.635
100000	0.858	-0.858	0.858	1.797	0.889	-0.889	0.889	1.862
120000	0.898	-0.899	0.899	1.883	0.927	-0.927	0.927	1.943

* $k_{xyz}=1$ (W/mK)

REFERENCES

1. ASHRAE Handbook of Fundamentals, 2001, Chapter 30 Fenestration, ASHRAE, GA.
2. Batechelor, G.K., 1954, "Heat Transfer by Free Convection across a Closed Cavity between Vertical Boundaries at Different Temperatures," Quarterly of Applied Mathematics, Vol. 12,no.3, pp. 209-233.
3. Bergholz, R.F., 1978, "Instability of Steady Natural Convection in a Vertical Fluid Layer," J. Fluid Mech., Vol. 84(4), pp.743-768.
4. ElSherbiny, S.M., Hollands, K.G.T., Raithby, G.D., 1982, "Effect of Thermal Boundary Conditions on Natural Vertical and Inclined Air Layers," J. Heat Transfer, Vol.104, pp. 515-536.
5. ElSherbiny, S.M., 1980, "Heat Transfer by Natural Convection across Vertical and Inclined Air Layers," Ph.D Thesis, Department of Mechanical Engineering, University of Waterloo.
6. ElSherbiny, S.M., Raithby, G.D., Hollands, K.G.T., 1982, "Heat Transfer by Natural Convection across Vertical and Inclined Air Layer," J. Heat Transfer, Vol. 104, pp.96-102.
7. Finlayson, E.U., Arasteh, D.K., Huizenga, C., Rubin, M.D., and Reilly, M.S., 1993, "WINDOW: Documentation of Calculation Procedures," Energy and Environmental Divison, Lawrence Berkeley Laboratory, Berkeley, California.
8. "Fluent Computational Fluid Dynamics Software Manual", Release 6.0, Fluent Inc.,2001.
9. Garnet, J.M., Fraser, R.A., Sullivan, H.F. and Wright, J.L., 1995, "Effect of Internal Venetian Blinds on Window Centre-Glass U-Values," Window Innovations '95, Toronto, pp 273-279.
10. Garnet, J.M., 1999, "Thermal Performance of Windows with Inter-Pane Venetian Blinds," M.E.Sc. Thesis, University of Waterloo, Waterloo, Ontario, Canada.
11. Hollands, K.G.T., Unny, T.E., Raithby, G.D., Konicek, L., 1976, "Free Convection Heat Transfer across Inclined Air Layers," J. Heat Transfer, Vol.98, No.2.
12. Holman, J.P., 1997, "Heat Transfer," 8th Edition, McGraw Hill, Toronto, 1997.
13. Incropera, F.P., Dewitt, D.P., 1996, Introduction to Heat Transfer, John Wiley & Sons, Inc.

14. Korpela, S.A., Lee, Y. and Drummond, J.E., 1982, "Heat Transfer through a Double Plane Window," *Transaction of the ASME Journal of Heat transfer*, Vol. 104, pp. 539-544.
14. Lai, B., 2004, "An Interferometric Study of Free Convective Heat Transfer in a Double Glazed Window with a Between-Panes Venetian Blind," M.E.Sc. Thesis, Ryerson University.
15. Lee Y., Korpela, S., 1983, "Multicellular Natural Convection in a Vertical Slot," *J. Fluid Mech.*, vol. 126, pp.91-121.
16. Machin, A.D., 1997, "An Experimental Study of Free Convective Heat Transfer From a Vertical Flat Plate in the Presence of Louvers," M.E.Sc Thesis, The University of Western Ontario.
17. Naylor, D. and Collins, M., 2004, "Evaluation of an Approximate Method for Predicting the U-Value of a Window with a Between-Panes Louvered Shade," *Proceedings of CHT-04, International Symposium on Advances in Computational Heat Transfer*, Norway.
18. Oosthuizen, P.H. and Naylor, D., 1999, *Introduction to convective Heat Transfer Analysis*, Mc-Graw-Hill, London.
19. Oosthuizen, P.H., and Naylor, D., "A Numerical Study of Free Convective Heat Transfer in a Parallelogram-Shaped Enclosure," *International Journal of Numerical Methods for Heat and Fluid Flow*, Vol. 4, pp. 553-559.
20. Phillips, J., "A numerical Study of the Effects of Venetian Blinds on Radiation and Convection Heat Transfer from a Window Glazing," M.E.Sc. Thesis, University of Western Ontario.
21. "Pella Doors and Windows", <http://pella.com>, Pella Corporation.
22. Raithby, G.D., Hollands, K.G.T., Unny, T.E., 1977, "Analysis of Heat Transfer by Natural Convection across Vertical Fluid Layers," *J. Heat Transfer*, Vol. 99, pp. 287- 293.
23. Shahid, H., 2003, "A Simplified Technique for Thermal Analysis of a Fenestration System with a Venetian Blind," M.Sc. Thesis, Dept. of Mechanical Engineering, Ryerson University.
24. Shahid, H., 2003, "A Simplified Technique for Thermal Analysis of a Fenestration System with a Venetian Blind," M.E.Sc. Thesis, Ryerson University.

25. Shahid, H., and Naylor, D., 2003, "Thermal Simulations of a Fenestration with Horizontal Venetian Blind," Proceedings of APM2002, 3rd International Conference on Computational Heat and Mass Transfer.
26. Shewen, E.C., 1986, "A Peltier Effect Technique for Natural Convection Heat Flux Measurement Applied to the Rectangular Open Cavity," Ph.D thesis, Department of Mechanical Engineering, University of Waterloo, Canada.
27. Shewen, E.C., Hollands, K.G.T., Raithby, G.D., 1996, "Heat Transfer by Natural Convection across a Vertical Air Cavity of Large Aspect ratio," J. Heat Transfer, Vol. 118, pp. 993-995.
28. Siegel, R., and Howell, J.R., 1972, Thermal Radiation Heat Transfer. McGraw-Hill, New York.
29. Vest, C.M., Arpaci, V.S., 1969, "Stability of Natural Convection in a Vertical Slot," J. Fluid Mech., Vol. 36, part 1, pp. 1-15.
30. Wright, J., 1996, "A Correlation to Quantify Convective Heat Transfer between Vertical Window Glazings," ASHRAE Transactions, 102(1), pp. 940-946.
31. Wright, J.L., Sullivan, H.F., 1989, "Natural Convection in Sealed Glazing Units: A review," ASHRAE Transactions 95(1), pp.592-603.
32. Wright, J.L., and Sullivan, H.F., 1992 "VISION3 Glazing System Thermal Analysis: Reference Manual, Advanced Glazing Laboratory," Department of Mechanical Engineering, University of Waterloo.
33. Wright, J.L., Sullivan, H.F., 1994, "A Two-Dimensional Numerical Model for Natural Convection in a Vertical Rectangular Window Cavity," ASHRAE Transactions, 100(2), pp. 1193-1206.